Palaeogeography, Palaeoclimatology, Palaeoecology 461 (2016) 401–417

Contents lists available at ScienceDirect

Palaeogeography, Palaeoclimatology, Palaeoecology

journal homepage: www.elsevier.com/locate/palaeo

A Multi-Proxy Analysis of two Loess-Paleosol Sequences in the Northern Harz Foreland, Germany

Lydia Krauß [a,*], Joerg Zens [a], Christian Zeeden [a], Philipp Schulte [a], Eileen Eckmeier [a,b], Frank Lehmkuhl [a]

[a] RWTH Aachen University, Department of Geography, Aachen, Germany
[b] Ludwig-Maximilians-University Munich, Department of Geography, Munich, Germany

ARTICLE INFO

Article history:
Received 7 May 2016
Received in revised form 1 September 2016
Accepted 2 September 2016
Available online 4 September 2016

Keywords:
Loess-paleosol-sequences
Last glacial maximum
Last cover loess
MIS 3 soil complex
Northern Harz foreland

ABSTRACT

Two loess-paleosol-sequences from the northern Harz foreland, Hecklingen and Zilly, have been investigated. In general, loess-paleosol-sequences represent valuable terrestrial archives of regional environmental and climatic conditions during past glacial periods. The study area is part of the northern European loess belt and was in the vicinity of the Scandinavian ice sheet during the Weichselian. Aiming towards a better understanding of the paleoenvironmental conditions during the Weichselian in an area close to the Scandinavian ice sheet, results from grain-size, geochemical (XRF, CNS), color and magnetic susceptibility measurements are combined. The findings demonstrate an increased input of aeolian material during the last glacial maximum and the last cover loess period, which is in accordance to the theory of drier and colder conditions during this time frame. Further, data reveal a strong input not only of loess but also of coarser material coming from a shorter distance during the last glacial maximum in both profiles. Material of the last glacial maximum clearly indicates a shift of wind direction towards easterly winds. In Hecklingen, an enhancement of coarser material has been observed within the recent soil and MIS 3 soil material. Since soil material that dates back to the MIS 3 is present in the profile, it can be assumed that surface processes were less intrusive during the MIS 3 and 2 than in e.g. the Lower Rhine Embayment and Saxony.
© 2016 Elsevier B.V. All rights reserved.

1. Introduction

Reconstructing environmental and climatic conditions of the past is crucial for understanding Earth's climate system of the past and present. For such reconstructions several types of geoarchives are available. Loess-paleosol-sequences (LPS) often represent the best accessible archive in terrestrial environments (e.g. Fischer et al., 2012; Fitzsimmons et al., 2012). Despite numerous attempts to define the term "loess", no universally accepted definition exists. This results and causes a various use of the term "loess" and loess-like sediments at the same time (see e.g. Pécsi and Richter, 1996; Smalley et al., 2011; Sprafke and Obreht, 2015). Here, loess is defined as an aeolian, homogeneous, predominately silt-sized, calcareous and yellowish loose sediment, which covers around 10% of the land surface on Earth (e.g. Muhs, 2007; Thome, 1998; Pécsi, 1990). As some people before and after him, Smalley (1966) defined four criteria that have to be fulfilled in order to result in a formation of LPS: (1) source material is required, (2) wind is needed to transport the material, (3) a trap where loess can accumulates has to be present, and (4) an adequate amount of time for the accumulation and post-depositional modification processes needs to be given. Usually loess accumulates in dry and cold environments. Soils develop on loess during warmer and moister periods. Due to changes of climatic and environmental conditions a series of loess and paleosols accumulates and develops, forming LPS. In comparison to deep-sea sediment and ice cores, LPS represent important archives of continental conditions, also close to archeological findings (Assallay et al., 1998; Frechen et al., 2003; Pye, 1996; Pye, 1987; Smalley, 1995; Wright, 2001; Kels and Schirmer, 2010).

The forty years of German separation complicated research on LPS in the northern Harz foreland. As a consequence, only small isolated investigations have been done in the northern Harz foreland mostly during the 1960s and 1970s from both former German states with a dissimilar range of methods applied, in comparison to intensively studied areas, like the Lower Rhine Embayment (e.g. Remy, 1960; Brunnacker, 1967; Paas, 1968; Schirmer, 2000; Kels, 2007; Fischer, 2010). Additionally, the region is close to the northern loess boundary, which restricts the research area to the north. Most research done in the northern Harz foreland focused on this transition zone, where Weichselian silt- and sand-sized aeolian sediments both occur (Poser, 1951). Investigations at the northern loess boundary have been done by e.g. Gehrt (1994), Gehrt and Hagedorn (1996) and Brosche and Walther (1978). Contributions from further east concerning the loess boundary are given by e.g. Schmidt (1971), Altermann and Fiedler (1975), Billwitz and Haase (1964), Göbeler (1966), Haase et al. (1970), Neumeister (1971) and Schmidt (1971). A number of isolated studies have been done in the

* Corresponding author.
E-mail address: Lydia.Krauss@geo.rwth-aachen.de (L. Krauß).

http://dx.doi.org/10.1016/j.palaeo.2016.09.001
0031-0182/© 2016 Elsevier B.V. All rights reserved.

eastern and southeastern Harz foreland by e.g. Kunert and Altermann (1965), Ruske and Wünsche (1961, 1964, 1968), Ruske et al. (1962), Neumeister (1966) and Göbeler (1966). An overview of the research done prior to 1970, covering the loess areas of the former GDR is given by Haase et al. (1970). Attempts to broaden the knowledge of the regional loess stratigraphy in the western Harz foreland studies on several LPS were initiated by Rohdenburg and Meyer (1966), Bork and Rohdenburg (1979), Ricken (1983) and Brosche and Walther (1991). Wagner (2011) recently analyzed the spatial distribution of loess and its derivates along the Weser-Aller catchment.

The first study which aimed to cover a larger area of the northern Harz foreland crossing the former border was done by Reinecke in 2006. For about ten years now no further intense research has been done in the northern and northeastern Harz foreland. In the eastern and southeastern Harz foreland and east of Leipzig new investigations have been conducted by Mania (2003), Mania and Altermann (2001), Baumgart et al. (2013), Kreutzer et al. (2012, 2014), Meszner et al. (2011, 2013) and Zech et al. (2013). Meszner et al. (2013) introduced a composite profile of Saxony which indicates strong erosion phases causing hiatuses, having large depositional gaps, e.g. a gap between ~35–65 ka.

In general, a stratigraphical classification of the last glacial cycle in Western and Central Europe is usually based on a locally valid nomenclature. This makes cross referencing challenging (e.g. Schönhals et al., 1964; Rohdenburg and Meyer, 1966; Brunnacker, 1967; Haesaerts et al., 1981; Schirmer, 2000; Bibus, 2002; Zens et al., 2016). For the northern Harz foreland a stratigraphical classification of the LPS was last done by Reinecke (2006). He tried to integrate the stratigraphies of the northern Harz foreland into the local Late Weichselian loess stratigraphies of Rohdenburg and Meyer (1966) and Semmel (1968). However, the lack of solid LPS exceeding 2.5 m of thickness makes a precise stratigraphical classification of the LPS challenging. Except the profiles in favorable relief positions (especially subrosion depressions) only a few LPS are known exceeding 2.5 m thickness (Brosche and Walther, 1991; Reinecke, 2006). Further, the Eltville tephra as an important marker within the Weichselian loess is missing. It is widely accepted that the LPS generally can only be placed into the Late and, if present, the Middle Weichselian without further subdivision (e.g. Merkt, 1968; Haase et al., 1970; Brosche and Walther, 1991; Gehrt, 1994; Feldmann, 2002; Reinecke, 2006). The first trials of narrowing down the age range of sediments at the northern loess boundary (OSL-/TL-dating) suggest that they date to the Weichselian Late Pleniglacial until Late Glacial (Hilgers et al., 2001). Ages generated by Reinecke (2006) for LPS close to the northern margin of the Harz Mountains suggest loess sediments to be partially of Middle Weichselian age.

In this paper two LPS initially introduced by Reinecke (2006) are discussed. They have been reinvestigated by using new analytical methods. The aim of this paper is the expansion of knowledge concerning the paleoenvironmental conditions during the last glacial period in an area close to the former Scandinavian ice sheet by applying grain-size, geochemical (XRF, CNS), color and magnetic susceptibility measurements. An equivalent multi-proxy approach has not been done before in this region.

2. Regional setting

The two profiles, Hecklingen (N 51°50.451′; E 11°31.580′; 106 m asl) and Zilly (N 51°56.280′; E 10°50.643′; 182 m asl), are located in the northern and northeastern Harz foreland (see Fig. 1) which represents a transition zone between the flat North German Basin and the Harz Mountains. The Hecklingen profile is located on a relative shallow angled slope which follows a northwest direction with a slope angle of 2.3°. The profile faces towards the southeast. In Zilly the slope follows a southwest direction with an angle of around 2°. The profile faces towards the east.

The climate of the northern Harz foreland gradually changes from sub-oceanic to sub-continental following a west-east gradient. Whereas in the western Harz foreland the mean annual precipitation can reach over 1000 mm, it drops below 500 mm in the eastern part of the northern Harz foreland due to the rain shadow effects caused by the Harz Mountains. The eastern part of the northern Harz foreland is part of the so-called Central German Arid Region where annual precipitation can even drop below 400 mm in drier years (Döring, 2004; Fabig, 2007; Haase et al., 1970; Krauß et al., 2013; Reinecke, 2006).

With a mean annual air temperature of ca. 9 °C the northeastern Harz foreland is one of the warmer regions in Germany. Excluding areas along the Rhine and its tributaries, there are only a few places with comparable high or higher mean annual air temperatures. Longer frost periods during winter time are rather the exception, resulting in mean monthly winter temperatures above 0 °C. July and August have similar mean temperatures with 18.4 and 18.3 °C which mark the middle of summer. In combination with low annual precipitation rates, the mild temperature regime causes a negative climatic water balance at least during drier years (Döring, 2004; Krauß et al., 2013).

The dominant wind direction is west-southwest and the secondary is from the east. On average, the winter is dominated by southwesterly to west-southwesterly winds with the highest frequency of occurrence in January. In summer a westerly to northwesterly wind direction is most frequent. In April and March easterly wind patterns dominate. During the more cyclonic weather phases (January–February and June–July) the easterly wind direction is weakest (Döring, 2004).

The northern Harz foreland is part of the Subhercynian Basin, which is bordered by uplifted bedrock. To the northeast it is limited by the Flechtinger-Rosslauer block and to the southeast and south by the Halle-Hettstedter mountain ridge and the Harz Mountains. To the northwest the basin is open. Generally, the basin is covered by Mesozoic and Cenozoic sedimentary rocks, mainly of shallow marine origin. Due to block faulting and salt tectonics, the formerly horizontally bedded Mesozoic layers are anticlinal in several places and show an almost exclusively southeast-northwest strike trend. The synclines between those anticlines are commonly filled with Cretaceous sediments beneath a Quaternary cover (see Fig. 2). This causes a slightly wavy surface appearance (Haase et al., 1970; Patzelt, 2003; Razinksi et al., 2008; Reinecke, 2006; Wagenbreth and Steiner, 1990).

In the northern Harz foreland Pleistocene deposits are mainly loose sediments, which vary in thickness and composition. Those sediments are primarily fluvial terraces, some lacustrine and (peri)glacial deposits of the Saalian and Weichselian glacial cycle (Litt and Wansa, 2008). Major rivers in the northern Harz foreland are the Oker River and the Ilse River as tributaries of the Weser River. The Aue River, the Holtemme River, the Bode River, the Selke River and the Wipper River are tributaries of the Elbe River. The closest river to Hecklingen is the Bode River 2.5 km north-east of the profile. The Zilly profile is within 0.4 km south to 1 km east of the Aue River. Even though those rivers are small, they developed large alluvial fans during the Quaternary. For more details, see Reinecke (2006) and Lehmkuhl et al. (2016).

The loess-covered areas are part of the Northern European loess belt. The northern edge of the loess distribution is characterized by the occurrence of both Weichselian silt- and sand-sized aeolian sediments. Gehrt (1994) found that this transition zone cannot be understood as a result of continuous sorting as Poser (1951) suggested, but as a result of multiple aeolian sorting phases, where sediments get increasingly sandier the younger they are. To the northeast the loess distribution is restricted by the river Elbe. To the south the Northern European loess belt is limited by the Central German uplands. Here the continuous loess cover disperses into separated loess basins where loess can only be found up to elevations between 400 and 500 m asl and is only present as reworked loess. The Weichselian loess of the northern and eastern Harz foreland surrounds the Harz Mountains in a 40 to 50 km wide belt (see Fig. 1). Generally, the thickness of the loess cover rarely exceeds 2.5 m. However, in unique settings (e.g. subrosion depressions) the thickness can reach several meters (Haase et al., 1970; Reinecke, 2006).

Recent soils developed on the loess cover are chernozems and regosols. In flood plains fluvisols are present, mainly derivatives of former

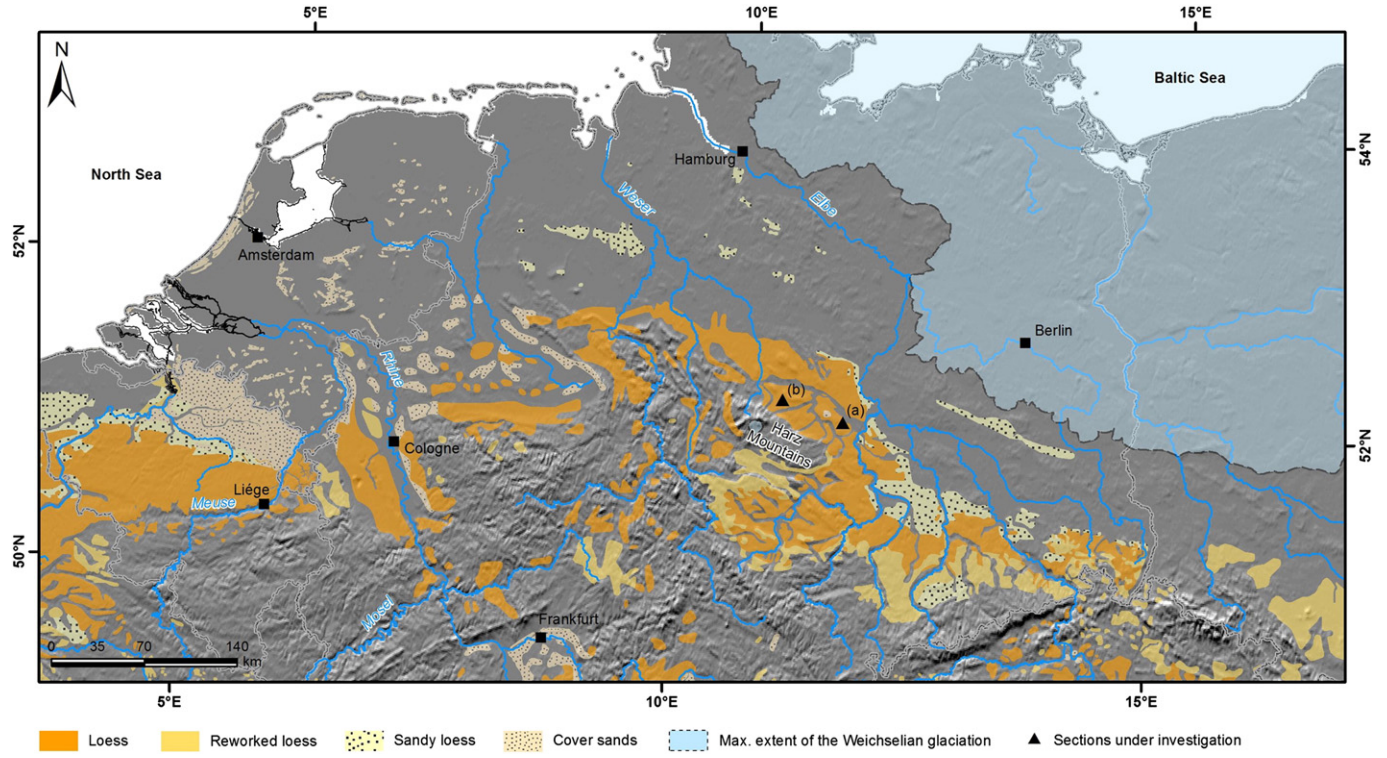

Fig. 1. Weichselian distribution of loess (orange), reworked loess (yellow), sandy loess (light yellow black dotted signature), cover sands (light brown dark brown dotted signature) (after Haase et al. (2007); modified by integrating data given by Zagwijn and Van Staalduinen (1975) and Haesearts et al. (2011) for the Netherlands and Belgium) in context of the maximum extent of the ice sheet during Weichselian glaciation (after Ehlers et al., 2004, 2011) in Central and Western Europe. Border of loess distribution is sharp due to Scandinavian ice sheet margin. Triangles mark the investigation sites (a) Hecklingen and (b) Zilly.

chernozems. Furthermore, on intensively used agricultural land anthrosols may occur. In higher elevations cambisols and luvisols can also appear. Due to the high soil quality of the loess covered areas, the land is predominantly used for agricultural purposes (USS Working Group WRB, 2015; LAGB, 2006; Zech et al., 2013).

3. Methods

3.1. Fieldwork

During June 2014 the Hecklingen and Zilly profiles were cleaned, documented and sampled for sedimentological analyses. Samples were continuously taken in a high resolution of 5 cm for multi-elemental (XRF), $CaCO_3$ content, environmental magnetic, color and grain-size distribution measurements. The generated datasets are available at http://dx.doi.org/10.5880/SFB806.28 and at http://dx.doi.org/10.5880/SFB806.27.

3.2. Grain-size analyses

In the laboratory all samples were dried at 35 °C, homogenized and sieved to <2 mm. For further analysis, 0.1–0.3 g of the finer grain fraction (<2 mm) were treated with 0.7 ml of a 30% hydrogen peroxide solution (H_2O_2) and exposed to 70 °C for several hours to remove the organic matter. This procedure was repeated up to three days until the sediment showed bleaching effects (Allen and Thornley, 2004). The particles were kept in suspension (to avoid the presence of aggregates and the formation of flocculation) by treating them with 1.25 ml of 0.1 M sodium pyrophosphate decahydrate ($Na_4P_2O_7x10H_2O$) for 12 h in an overhead shaker (DIN ISO 11277, 2002; Schulte et al., 2016).

Particle-size measurements were done with a Laser Diffraction Particle Size Analyzer (LS13320, Beckman Coulter). The analyzer gives out 116 logarithmic grain-size classes within a range of 0.04–2000 μm with a precision below 2% CV (coefficient of variation). Each sample was measured at two different concentrations twice to enhance the accuracy and averaged afterwards (Pye and Blott, 2004). For calculating the grain-size distribution the Mie theory was applied (Fluid RI: 1.33; Sample RI: 1.55; Imaginary RI: 0.1) (ISO 13320-1, 1999; Özer et al., 2010; Schulte et al., 2016). If the LS 13320 with additional PIDS technology is used for laser diffraction measuring and the Mie theory (with a useful complex refraction index (m = n − ki)) is applied for grain-size calculation (Schulte and Lehmkuhl, 2016), the phenomenon of systematic underestimation of the clay fraction is negligible in loess sediments. The grain-size classes were defined after the ISO standard 14688 (2002) (see also Blott and Pye, 2012). Classes were divided as followed: <0.2 μm for fine clay, <0.63 μm for middle clay, <2 μm for coarse clay, <6.3 μm fine silt, <20 μm for middle silt, <36 μm for lower coarse silt, <63 μm for upper coarse silt, <200 μm for fine sand, <630 μm for middle sand and <2000 μm for coarse sand. The grain-size index (GSI), first introduced by Rousseau et al. (2002), as an index for wind dynamics and atmospheric dust, was calculated by GSI = percentage of the fraction between 26 and 52.6 μm / percentage of the fraction finer than 26 μm (Antoine et al., 2009; Rousseau et al., 2007). The U-ratio, established by Vandenberghe (1985), as an index for shifts between warm and cold periods through low to high wind dynamic changes, was calculated by U-ratio = percentage of the fraction between 16 and 44 μm / percentage of the fraction between 5.5 and 16 μm (e.g. Vandenberghe et al., 1997; Vandenberghe and Nugteren, 2001). A recent overview on loess-grain-size proxies is given by Újvári et al. (2016).

3.3. Geochemical analyses

The sample material was sieved at 63 μm and the fine (silt and clay) fraction was dried for 12 h at 105 °C. An eight gram aliquot of each sample was mixed with 2 g of wax binder (Fluxana Cereox), homogenized and pressed into a pellet at 19.2 MPa for 120 s. To determine the element concentrations, samples were analyzed using an energy

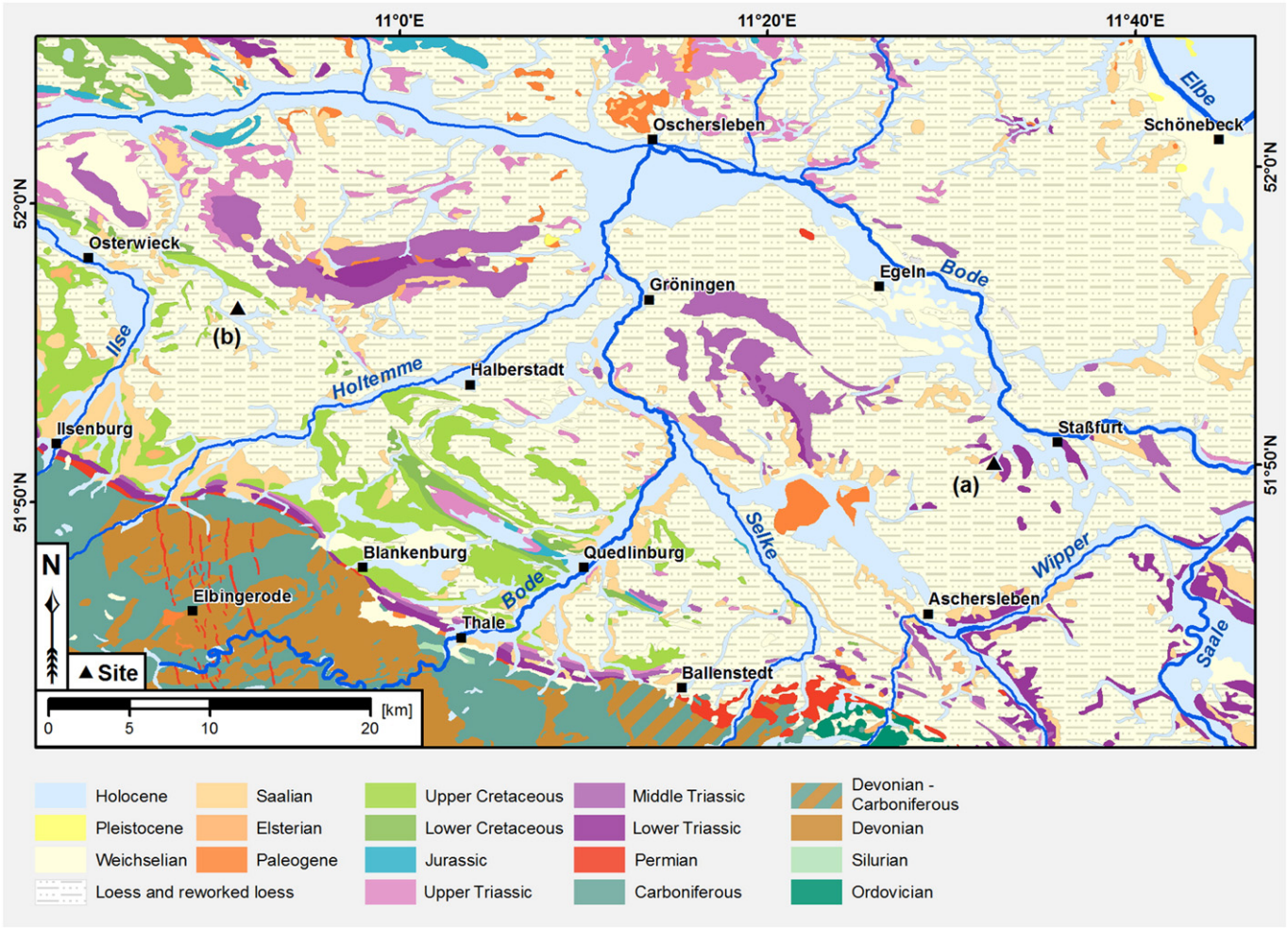

Fig. 2. Geological map of the northern Harz foreland (section generated and modified after General Geological Map of Germany 1:200,000 (GÜK200), Bundesanstalt für Geowissenschaften und Rohstoffe (BGR) revised, 2015). Triangles mark the investigation sites (a) Hecklingen and (b) Zilly.

dispersive X-ray fluorescence (ED-XRF) spectrometer (SPECTRO XEPOS, SPECTRO Analytical Instruments GmbH). Oxides were calculated by using element specific conversion constants. The chemical index of alteration (CIA) (Nesbitt and Young, 1982) was calculated as CIA = $[Al_2O_3 / (Al_2O_3 + Na_2O + CaO^* + K_2O)] * 100$ (in molar proportions; CaO^* refers to silicatic Ca) and the chemical proxy of alteration (CPA) was calculated as CPA = $[Al_2O_3 / (Al_2O_3 + Na_2O)] * 100$ (in molar proportions). For detailed information on weathering indices, in particular CIA and CPA, the reader is referred to studies conducted by e.g. Buggle et al. (2011), Cullers (2000), McLennan (1993) and Schatz et al. (2015).

The calcium carbonate ($CaCO_3$) content was determined with a calcimeter working in accordance to the Scheibler method. By adding a 10% hydrochloric acid solution to the sample material the calcium carbonate converts into carbon dioxide (CO_2) resulting in changing pressure conditions in the apparatus. The quantity of this change is used to calculate the $CaCO_3$ content (Schaller, 2000; ISO 10693, 1995).

3.4. Color measurements

The color of every sample was measured in triplicates on dry, homogenized and sieved (< 2 mm) material with a spectrophotometer (Konica Minolta CM-5). The spectrophotometer detected the diffused reflected visible light in the range 360 to 740 nm under standardized observation conditions (2° Standard Observer, Illuminant C). The results were transferred into Munsell values and into the CIELAB Color Space System (CIE 1976) with the Software SpectraMagic NX (Konica Minolta). The extinction of light or luminance is indicated by the L^* values, on a scale from 0 (absolute black) to 100 (absolute white). Further, the CIELAB values display color as chromaticity coordinates on red-green (a^*) and blue-yellow (b^*) scales (Eckmeier et al., 2010; Gocke et al., 2014; Vlaminck et al., 2015). Color data was plotted after Zeeden et al. (2016) and used as a background in most proxy data graphs (see Figs. 3, 5, 6, 8).

3.5. Environmental magnetic analyses

Samples were dried at 35 °C, roughly ground, packed into small plastic boxes and manually compressed. To avoid particle movement during the measurement, cotton wool was packed to fill the boxes.

Samples and 10 empty boxes were weighed. A MAGNON Susceptibility Bridge (MAGNON, Dassel, Germany) was used for measurements at frequencies of 310 and 3013 Hz in a static field of 320 mA/m. For the determination of the magnetic susceptibility of the plastic boxes the 10 empty boxes were measured and averaged. The data were corrected for drift, the effect of the boxes (weak diamagnetism) and normalized to density. Here, the magnetic susceptibility is given as mass specific susceptibility (χ) in m^3/kg. The frequency dependence [%] was calculated as $\chi_{fd} = (\chi_{lf} - \chi_{hf}) / \chi_{lf} * 100$ (e.g. Thompson and Oldfield, 1986).

3.6. Luminescence dating

Infrared stimulated luminescence (IRSL) measurements of the Hecklingen and Zilly sections were carried out in the Cologne Luminescence Laboratory in 2003/04 by A. Hilgers. Ages were published by

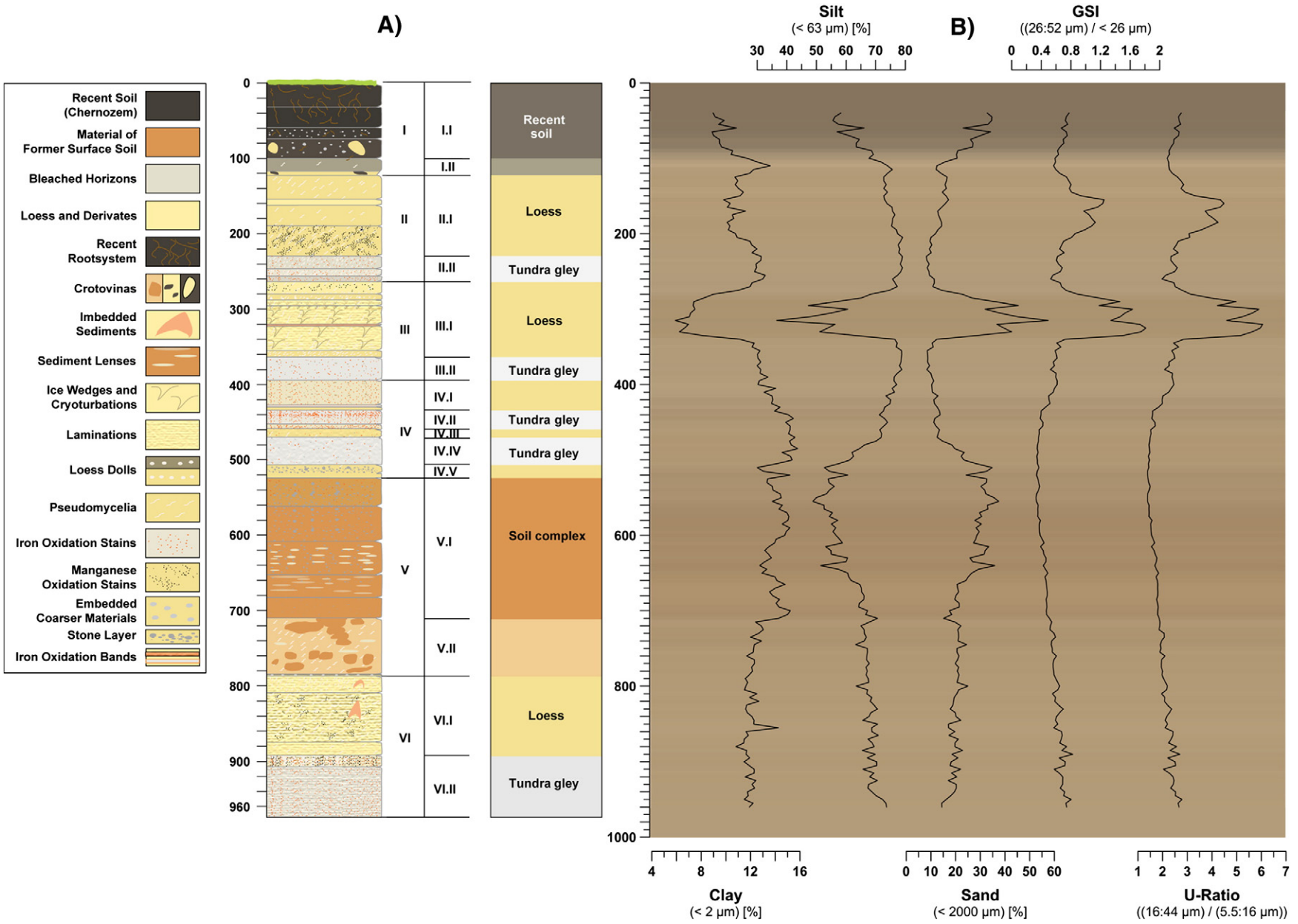

Fig. 3. Hecklingen (from left to right): A) plotted against depth [cm] a detailed semi-generalized stratigraphy with features (legend on the left) observed in the field, division of sequence into units based on proxy-data and simplified lithology based on units; B) main grain-size classes (clay, silt, sand), GSI and U-Ratio plotted against depth [cm] (with color data plotted in the background).

Reinecke (2006) without additional information concerning the dating procedure. In this study, the existing data are reevaluated and a short overview of the recently applied methods is provided including their results. The presented ages differ from previous published data due to using a different integration interval and a more recent age model.

The sample preparations for polymineral fine-grains (4–11 μm) were made according to the procedure presented by Frechen et al. (1996). Luminescence measurements were carried out on a Risø TL-DA-12 reader stimulating with infrared LEDs (880 ± 80 nm) and irradiating with a $^{90}Sr/^{90}Y$ beta source. The luminescence signals were detected passing a filter combination of a Schott BG39, Schott GG400 and Corning 7-59. For equivalent dose (D_e) measurements, the signal of the first 4.8 s was used after subtracting the background of the last 20 s. The single aliquot regenerative dose protocol (Murray and Wintle, 2000) modified for polymineral sample for 50 °C stimulation temperature was applied (Wallinga et al., 2000). All measurements were carried out at a preheat temperature of 270 °C. The central age model (CAM) was used for calculating the D_e (Galbraith et al., 1999). Fading correction methods were not applied.

The external dose rate was measured using high-resolution γ-spectrometry. The gravimetric water content was determined after drying and an uncertainty of 5% was assumed. Sample Heck-1 and all samples from Zilly yielded strongly reduced water contents below 4% compared to remaining loess samples with 10–16%. Therefore, an average water content of 12.5 ± 5% was estimated. Dose rate conversion factors from Guérin et al. (2011) and beta attenuation factors from Brennan (2003) were used. The internal beta dose rate was considered to be deriving from a potassium content of 12.5 ± 0.5% (Huntley and Baril, 1997). The α-efficiency of 0.07 ± 0.02 was assumed according to Preusser et al. (2005). The cosmic dose rate was calculated after Prescott and Hutton (1994). The total dose rate and the final age were determined with the DRAC online tool V1.1 (Durcan et al., 2015).

4. Results

4.1. Hecklingen

4.1.1. Stratigraphy

The Hecklingen profile is divided into six units based on field observations and the proxy results (see Fig. 3A). Several studies show a large difference between IRSL50 ages and fading corrected ages for loess from the same time slot leading to age underestimations of 4 to 6 ka (Frechen and Schirmer, 2011; Schmidt et al., 2011; Zens et al., 2016). Since no fading correction methods have been applied, minimum ages can be assumed (see Table 1). A parallelization of the profile to Reinecke's (2006) findings is given in Fig. 9.

The bottom of the sequence is marked by *unit VI.II*. The material is bleached, resulting in a grey appearance with red oxidation stains and pseudomycelia, typical for a so-called tundra gley. The lowermost age very likely puts the tundra gley into MIS 4 with a minimum age of 61.9 ± 4.7 ka. *Unit VI.I* is a loess layer showing a partially strong lamination and black-brownish manganese oxidation stains. *Unit V.II* is a truncated soil layer with crotovinas containing the soil material of the soil complex above. *Unit V.I* is an almost 2 m thick complex of brownish red soil material. A minimum age of 48.5 ± 3.8 ka below and 51.5 ± 4.5 ka within the upper part of the soil complex indicate a relation to MIS 3. The upper half contains more gravel-sized particles than the lower part where several silt and clay lenses were observed in the field. *Unit IV.V* was identified as a stony loess layer containing abundant gravel. *Unit IV.III* is a small loess layer separating the tundra gleys *unit IV.II* and *IV.IV*. *Unit IV.IV* is greyer with only a few oxidation stains but relatively frequent pseudomycelia features. *Unit IV.II* is a further tundra gley according to strong bleaching and abundant red oxidation stains within the layer. *Unit IV.I* is another loess layer with partially red iron oxidation stains. *Unit III.II* is the second uppermost tundra gley, based on reduction and oxidation features visible in the field. The ages 23.1 ± 1.8 ka and 22.9 ± 1.8 ka place *unit III.I* into the time of the last glacial maximum (LGM). The timing of the LGM was constrained by Clark et al. (2009) as occurring from 26.5 to 19.0 ka using relative sea level (RSL) data. The laminations, cryoturbation features and ice wedges within the unit support the time frame of the LGM. The material of *unit II.II* is bleached with red oxidation stains and pseudomycelia and marks the uppermost tundra gley of the sequence. Based on the uppermost age of 17.8 ± 1.4 ka *unit II.I* is part of the last cover loess with several pseudomycelia within the upper part and additional manganese oxidations stains in the lower part. *Unit I* represents the recent soil with a strong rooting within the first 40 cm and a chernozem-like appearance. Until 1.2 m depth several transition horizons with less rooting but large crotovinas are present.

4.1.2. Grain-size distributions within the profile

Fig. 3B shows the evolution of the three main grain-size classes (clay, silt, sand), GSI and U-Ratio throughout the sequence of Hecklingen. The figure in Appendix 1 shows a further separation of the grain-size classes into fraction subunits. The grain-size density distribution curves of the defined stratigraphic units are given in Fig. 4.

The silt content at the bottom of *unit VI.II* is higher than 70% while the clay content and sand content are below 15% (see Fig. 3B and Appendix 1). At the boundary between *unit V.I* and *V.II,* the values of clay-sized particles are strongly increasing. *Unit V.I* has the highest levels of fine and middle clay-sized particles compared to the other units of the profile. The middle and coarse sand fraction is oscillatory but increasing towards *unit IV.V*. Within *unit IV* particles with sizes below 6.3 μm and above 200 μm decrease again whereas mainly coarse silt increases towards the top. The strongest changes in fraction composition throughout the profile occur in *unit III.I*. Above 3.40 m depth the grain-size composition changes. Up to 58% of the grain-size fraction lies within the range of sand-sized particles. In comparison to *unit V.I* where changes in grain-size distribution were mainly driven by coarse and middle sand here the whole fraction changes. While the content of particles with sizes below 36 μm is reduced by 43%, the particles larger than 36 μm occupy up to 78% of the fraction (see Figs. 3B, 4B and

Table 1
Summary of luminescence ages resulting from dose rate calculation based on radionuclide concentrations from laboratory gamma spectrometry and equivalent dose (De) determination from 'single aliquot regenerative dose' measurements.

	Laboratory code	Sample code	U (ppm)	Th(ppm)	K (%)	Depth (m)	Dose rate (Gy ka)	Equivalent dose (Gy)	IRSL age (ka)
Hecklingen	C-L1305	HCK-1	2.30 ± 0.13	7.73 ± 0.58	1.41 ± 0.03	1.4	3.16 ± 0.18	56.0 ± 3.0	17.8 ± 1.4
	C-L1306	HCK-2	2.50 ± 0.21	9.30 ± 0.51	1.50 ± 0.03	2.35	3.46 ± 0.20	79.4 ± 4.2	22.9 ± 1.8
	C-L1307	HCK-3	2.41 ± 0.13	9.64 ± 0.59	1.52 ± 0.03	3.55	3.44 ± 0.19	79.3 ± 4.2	23.1 ± 1.8
	C-L1308	HCK-4	2.22 ± 0.09	8.76 ± 0.54	1.47 ± 0.03	5.25	3.24 ± 0.18	166.9 ± 11.1	51.5 ± 4.5
	C-L1309	HCK-5	2.15 ± 0.18	8.06 ± 0.46	1.42 ± 0.03	7.75	3.11 ± 0.18	150.6 ± 8.1	48.5 ± 3.8
	C-L1310	HCK-6	1.57 ± 0.12	6.62 ± 0.37	1.28 ± 0.03	8.55	2.55 ± 0.14	157.7 ± 8.5	61.9 ± 4.7
Zilly	C-L1386	ZIL-1	2.28 ± 0.28	9.00 ± 0.50	1.79 ± 0.04	0.8	3.66 ± 0.20	55.3 ± 2.9	15.1 ± 1.1
	C-L1387	ZIL-2	2.20 ± 0.10	7.92 ± 0.61	1.59 ± 0.03	1.35	3.32 ± 0.18	50.4 ± 2.7	15.2 ± 1.1
	C-L1388	ZIL-3	2.28 ± 0.08	7.98 ± 0.52	1.51 ± 0.03	2.28	3.27 ± 0.18	50.1 ± 2.6	15.4 ± 1.2
	C-L1389	ZIL-4	2.44 ± 0.20	8.61 ± 0.53	1.55 ± 0.03	2.44	3.42 ± 0.19	54.1 ± 2.8	15.8 ± 1.2

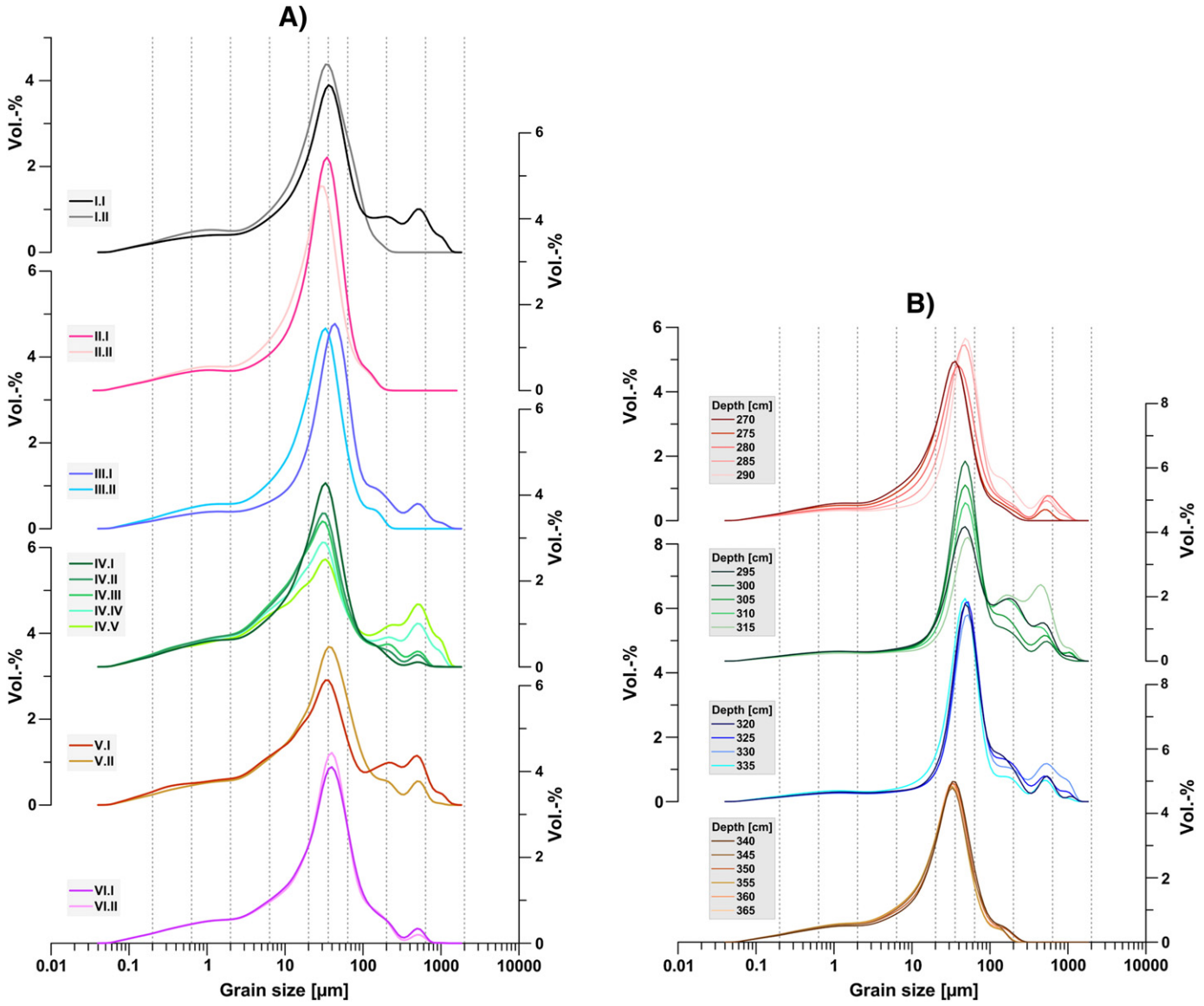

Fig. 4. Hecklingen (from left to right): A) grain-size density distribution curves of the defined units; B) unit III.I detailed grain-size distribution.

Appendix 1). In *unit II.II* the grain-size distribution shifts to higher values of particles below 36 µm in size again, containing no coarse and middle sand-sized particles anymore. Within *unit II.I* upper coarse silt is enhanced while particles below 36 µm of size are reduced. In *unit I.II* the clay and silt values are elevated once more. In *unit I.I* the sand fraction is increasing again to around 35%, which is mostly driven by relative high levels in coarse and middle sand (see Fig. 3B and Appendix 1).

The GSI and the U-ratio (Fig. 3B) behave similarly by having two maxima. From the bottom to the top, the first one occurs in *unit III.I* and is stronger than the second one. The second maximum occurs within *unit II.I*, where the GSI reaches values between 1.23 and 0.8, and the U-ratio values lie between 4.5 and 2.85. Throughout the rest of the profile the GSI and U-ratio vary slightly.

In Fig. 4A the grain-size distribution curves of the identified units are displayed. The main characteristics of all units are similar. They all have a dominant well-sorted silt component with a modal peak between around 30–40 µm. However, as shown in Fig. 4B the whole grain-size distribution in *unit III.I* temporarily shifts towards the coarser fraction. Especially the modal peak shifts to 55 µm. Further, all units have a very low clay fraction and show a second but smaller peak within the sand fraction but with varying amounts and modal values. *Unit IV.V* has the "weakest" dominant peak in silt-sized particles compared to the second peak in the sand-sized fraction and *unit II* contains no middle and coarse sand fraction at all.

4.1.3. Weathering indices and color properties

Fig. 5 shows the weathering indices, color properties and magnetic susceptibility features of the profile plotted with depth and in context of the identified stratigraphic units.

In *unit VI,* the a* value increases notably while the other indices are rather constant. At the border between *unit V.I* and *V.II* the values of Rb/Sr, Ba/Sr, CIA, CPA, a* and b* are enhanced whereas the $CaCO_3$ content suddenly drops. Within *unit V.I* Rb/Sr, Ba/Sr, CIA, CPA, Fe_2O_3, a* and b* are highest in context of the whole profile. In contrast, the $CaCO_3$ content is lowest in *unit V.I.* Within *unit IV* values of Rb/Sr, Ba/Sr, CIA, CPA, Fe_2O_3, a* and b* are higher in *subunits IV.II* and *IV.IV* compared to the other subunits. Mn/Fe and $CaCO_3$ have rather low amounts in IV.II and IV.III. In *unit III.II* Rb/Sr and Ba/Sr values are elevated. In *unit III.I,* the $CaCO_3$ content is reduced. The Fe_2O_3 content strongly decreases, too, but a* behaves conversely and has high values. Additionally, the material is darker, as seen in the L*. Towards *unit II.II*, Mn/Fe, a* and b* suddenly decrease while Fe_2O_3, L* and the mass specific susceptibility are elevated. Within *unit II.I*, a* values, $CaCO_3$ and Mn/Fe increase towards the top of the unit. Rb/Sr, Ba/Sr, CIA and CPA indices are also

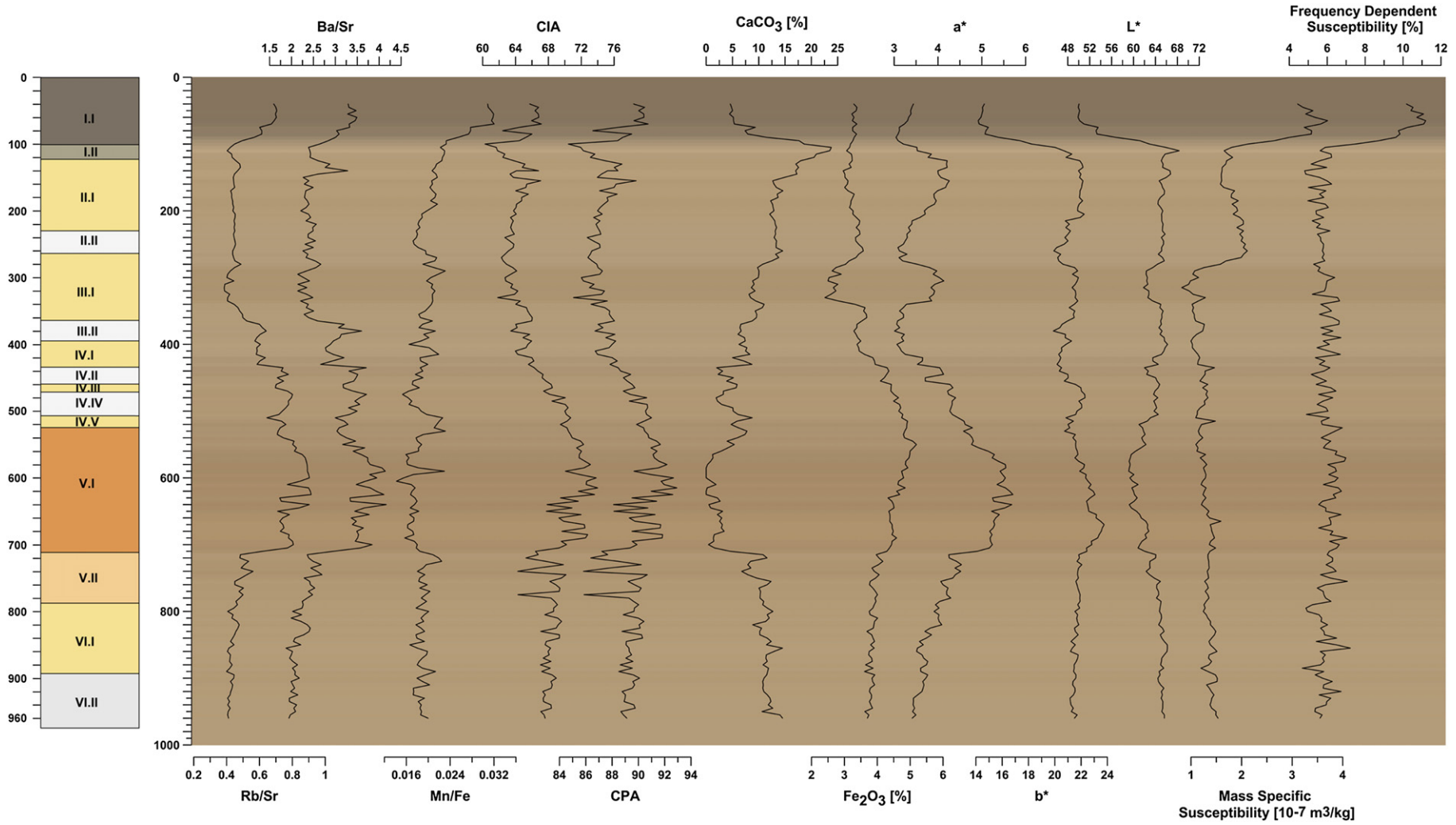

Fig. 5. Hecklingen (from left to right): Weathering indices, color data and magnetic susceptibility in relation to the simplified lithology based on defined units, plotted against depth [cm] (with color data plotted in the background).

elevated within the upper part of *unit II.I*. The mass specific susceptibility decreases towards *unit I.II* with a stronger decrease in the upper part of *unit II.I* and stays then relatively constant until *unit I.II*. In *unit I.II* this relationship is reversed. In *unit I.I,* the ratios Rb/Sr, Ba/Sr, Mn/Fe, CIA, CPA have strongly elevated values, whereas $CaCO_3$, redness-index (a*), b* and lightness-index (L*) have rather low quantities. The mass specific and frequency dependent susceptibility show the strongest enhancement in *unit I.I* when put into context of the whole profile.

4.2. Zilly

4.2.1. Stratigraphy

Reinecke published ages for the sequence of Zilly in 2006. He took OSL-samples up to a depth of 2.44 m (see Table 1). The recalculated youngest ages are between 15.1 ± 1.1 ka (0.80 m) and 15.8 ± 1.2 ka (2.44 m). The recent field observation and sedimentological proxies indicate that not the same sequence was sampled, since Reinecke (2006) only identified a 3 m thick last cover loess layer without variations in the field, which is supported by his data. In the present study several layers were identified, which are divided into three major units following the field observation and sedimentological proxies (see Fig. 6A).

Unit III is the suspected LGM loess possibly containing an intercalated bleached horizon. The material of *unit III* is completely laminated with stronger lamination at the top (see Fig. 6A). *Unit II* is believed to be the last cover loess with two intercalated bleached horizons which are assumed to be tundra gleys. The tundra gley *unit II.IV* is weakly laminated. The loess material of *unit II* partially includes pseudomycelia and manganese oxidation stains. Additionally, *unit II.I* includes bigger carbonate concretions (1–2 cm diameter). *Unit I* represents the recent soil with a strong rooting within the upper 25 cm and several transition horizons below. A parallelization of the profile to Reinecke's (2006) findings is given in Fig. 9.

4.2.2. Grain-size

Fig. 6B shows the behavior of the three main grain-size classes (clay, silt, sand), GSI and U-Ratio throughout the sequence of Zilly. The figure in Appendix 2 shows a further separation of the grain-size classes into subunits. The grain-size density distribution curves of the defined stratigraphic units are given in Fig. 7.

In *unit III.III* silt-sized particles occupy >70% of the fraction with highest amounts at 4.30 m depth decreasing towards *unit III.II*. Sand varies between 12 and 17% with lowest amounts at 4.30 m (see Fig. 6B). The clay content is relatively constant at around 11% throughout *unit III* except at 4.15 m depth where clay occupies 13.9% of the fraction. In *unit III.I* the sand fraction occupies up to 31% of the fraction at the disadvantage of silt. Within *unit II.IV,* the clay and sand fraction have declining amounts towards *unit II.III*. Within *unit II* the fraction below <36 μm increases towards the top of the unit. In *unit I.I,* clay values are highest with a maximum of 14.1% at 45 cm depth.

The GSI and the U-ratio in Fig. 6B behave similar, having two main increases. The first one is in *unit III.II* at 4.1 m depth. The second peak is in *unit II.III* having a maximum at 2.7 m depth with 1.03 for GSI and 3.49 for U-ratio.

In Fig. 7 the grain-size distribution curves of the identified units are displayed. All units have in common that the dominating components are silt-sized particles. Further, all units have a second peak within the sand fraction, which is strongest developed in *unit III*.

4.2.3. Weathering indices and color properties

Fig. 8 shows the weathering indices, color properties and magnetic susceptibility features of the sequence plotted with depth in connection with the defined stratigraphic units.

The strongest changes of the weathering indices, the color data and magnetic susceptibility are between *unit I* and the rest of the profile. The indices stay relatively constant throughout the rest of the profile, only CPA and CIA have slightly elevated values within *unit III* and *unit II.IV*. Between *unit II* and *unit I* Rb/Sr, Ba/Sr, CPA, CIA, Fe_2O_3 and a* values strongly increase while the $CaCO_3$ content is strongly reduced by 14.5% to around 0%. L* declines, too, but not as strongly as $CaCO_3$. Rb/Sr and Ba/Sr have high values in *unit I*. Rb/Sr slightly increases further towards the top of *unit I*, while Ba/Sr has relative constant values throughout the unit. CPA and CIA are highest in *unit I.III*. Fe_2O_3, L*, a* and b* values are relatively constant within the lower part of *unit I* but decrease between *unit I.II* and *unit I.I* towards the top. The Mn/Fe ratio, mass specific and frequency dependent susceptibility decrease within the lower part of *unit I* but strongly increase again towards the top starting at the boundary between *unit I.II* and *unit I.I*, having highest values in *unit I.I*.

5. Discussion – interpretation of the data

5.1. Hecklingen

As already indicated by field observations, the Hecklingen profile comprises several phases of environmental and climatic conditions during the Middle and Late Weichselian Glacial (see Figs. 3, 4, 5).

The clearly identified bleached horizon (tundra gley) at the bottom of the sequence (*unit VI.II*) is not identifiable in any of the investigated proxies. Relative to the material above, no changes in the geochemical, color and grain-size composition display the tundra gley by increased weathering.

The smooth transition between *unit V.II* and *VI.I* displayed by all proxies indicates a relative stable phase of loess accumulation prior to a soil formation (Figs. 3, 4A, 5). *Unit V.II* is not to be seen as a transition zone from loess sediment below to the soil material above. The strong cut in the geochemical ratios Ba/Sr and Rb/Sr (Fig. 5), also in the grain-size distribution heatmap (Appendix 4) suggest that the former soil was eroded leaving a truncated transition zone with crotovinas (*unit V.II*). The soil material above (*unit V.I*) seems not to be in-situ. It is rather redeposited soil material, probably belonging to the same phase of soil formation as the truncated transition zone below. The recalculated IRSL50 ages of Reinecke (2006) show similar ages for the soil material and the loess material below the truncated transition zone, and the fillings within the crotovinas appear to be the same material as the soil material above. Further, the weathering indices and the clay content are strongly varying within the soil material having highest values between 5.50 and 6.00 m depth, suggesting pedogenic overprinting within that area (Fig. 5 and Appendix 1, 5). This indicates the presence of at least one further soil formation phase during MIS 3 in Hecklingen, which overprinted the signal of the previously accumulated soil sediment. The smooth decline in weathering indices towards the top of *unit V.I* suggests decreasing pedogenesis. The gravel layer (*unit IV.V*) above soil material speaks to a further erosion phase (Boenigk and Frechen, 2001; Frechen et al., 1999; Marković et al., 2011). Ages support that there has been strong erosion during a late phase of MIS 3, causing this unconformity.

The identified bleached layers (tundra gleys) of *unit IV* and *unit III* are supported by the weathering indices Rb/Sr, Ba/Sr, CPA and CIA through higher values and by reduced amounts of $CaCO_3$, displaying hydromorphic conditions and leaching. The layers are likely connected to a warmer and moister phase (in comparison to very cold and dry conditions during interglacials), since the material is greyish and bleached, which is usually caused by repeated thawing of permafrost soils in combination with poor drainage (e.g. Antoine et al., 2009; Antoine et al., 2001; Terhorst et al., 2001; Vandenberghe et al., 1998; Vandenberghe and Nugteren, 2001; Van Vliet-Lanoë, 1998; Van Vliet-Lanoë, 1989).

The strong modification in grain-size distribution (Figs. 3B, 4B) within *unit III.I* is interpreted as a result of changes in wind dynamics. The shift of the grain-size mode of up to 20 μm towards the coarser range indicates a different source material during the LGM. While there are secondary influences present within the other units, the shift of the whole grain size distribution speaks for overall modifications of the primary

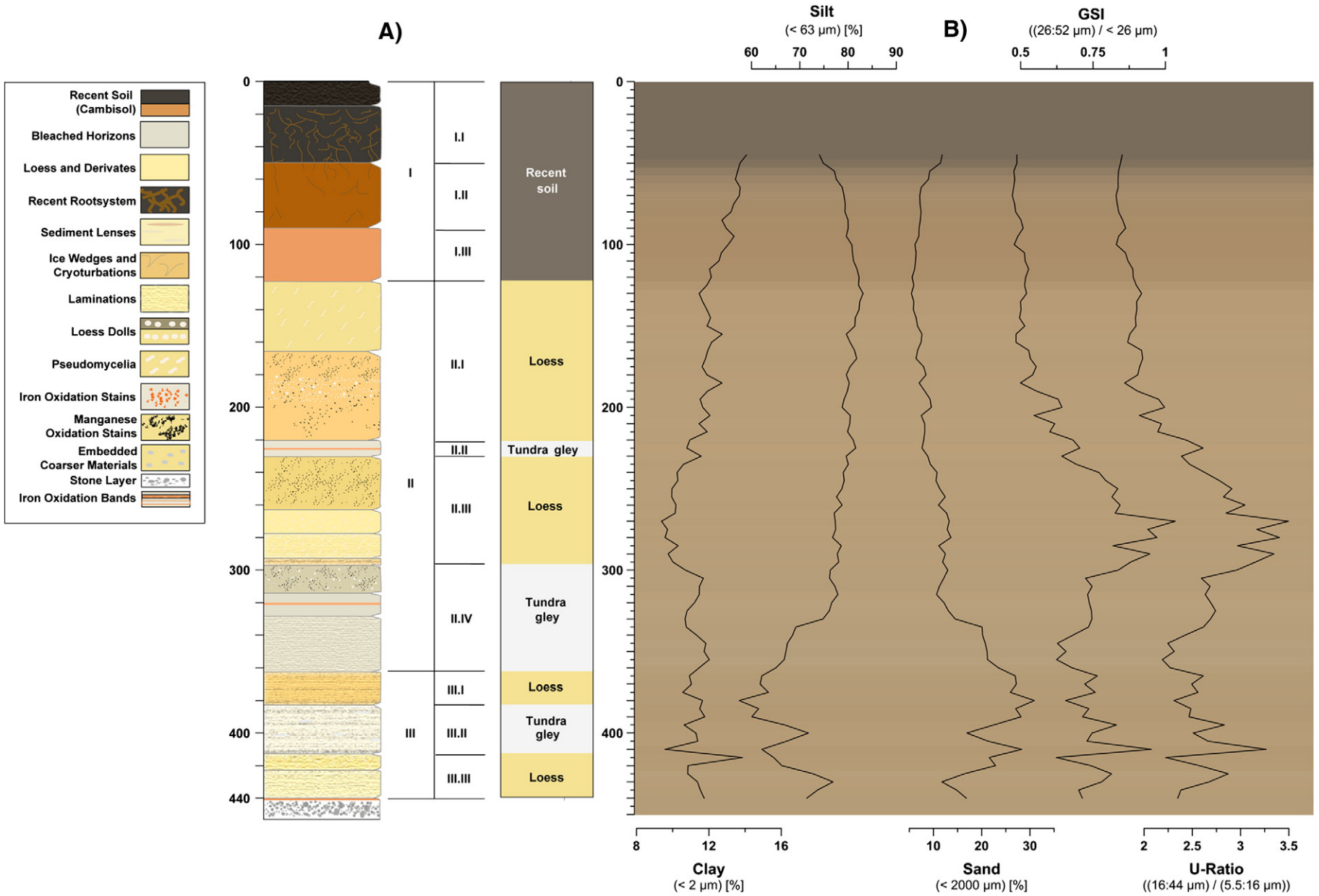

Fig. 6. Zilly (from left to right): A) plotted against depth [cm] a detailed semi-generalized stratigraphy with features (legend on the left) observed in the field, division of sequence into units based on proxy-data and simplified lithology based on units; B) main grain-size classes (clay, silt, sand), GSI and U-Ratio plotted against depth [cm] (with color data plotted in the background).

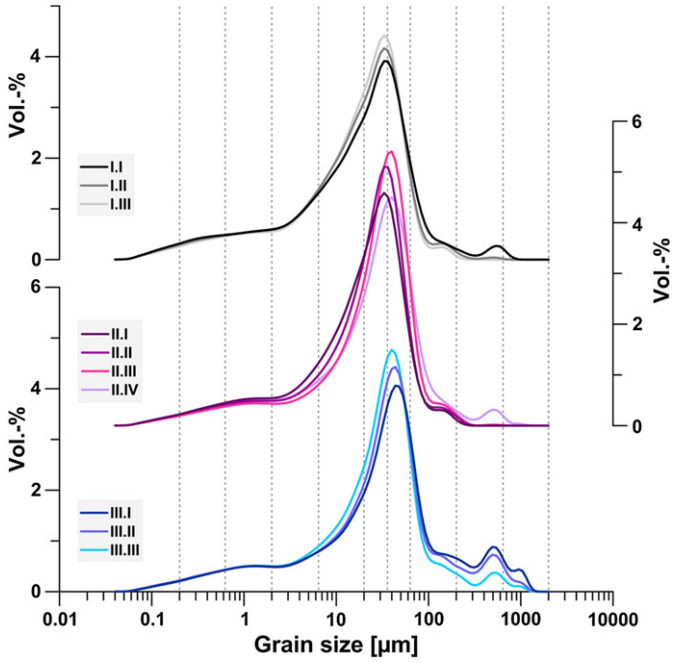

Fig. 7. Zilly grain-size density distribution curves of the defined units.

processes in connection with changes of the general wind direction. The high values of sand and upper coarse silt point to the presence of sediment derived from nearby areas (Fig. 4B). Those short distance transport processes include creep and saltation. Sandstones of the Triassic Buntsandstein are exposed within 0.5 km north and east of the profile (Fig. 2). They appear to be a likely source material for the high sand input phase in Hecklingen. Renssen et al. (2007) came to the conclusion that it is very unlikely that shifts in wind direction during the LGM occur for the most parts of Europe. New paleoclimate simulations by Ludwig et al. (2016) do suggest that only in Western Europe westerly winds got stronger during the LGM. For Central Europe though (including the northern Harz foreland) their modelling shows a shift towards southerly and easterly circulation weather types (CWTs). Ludwig et al. (2016) attribute this to the Scandinavian ice sheet and the corresponding formation of a strong anticyclone. This supports the findings by Dietrich and Seelos (2010) and Römer et al. (2016) for the Dehner Maar (Eifel Mountains) using heavy mineral analysis of sediment cores. Their records suggest strong easterly winds during the LGM. Consequentially, looking at the grain-size components, the Hecklingen profile seems to display strong easterly winds with several dust storm events during the LGM as well. Antoine et al. (2009) identified phases with high GSI and high values of fine sand events with high loess input (LE). In the Nussloch section, they revealed a high conformity of maxima in aridity and wind intensity (characterized by high amounts in GSI and sand fraction). Therefore, the high values of GSI and U-ratio within *unit III.I* support the theory of a phase with enhanced (aeolian) input of coarser material under dry conditions. However, due to the high medium and coarse sand content, surface runoff events cannot be excluded. Slope wash starts at an angle around 2° and since the slope angle in Hecklingen is 2.3° surface runoff could have occurred during heavy rainfall events. Nevertheless, the redness-index (a*) supports the hypothesis of wind direction changes by high values where iron oxide behaves contrary and has an unexpected decrease (see Fig. 5). High a* values are mostly caused by enhanced iron oxides in a sediment as a result of pedogenic processes under warmer and moister conditions (Kehl et al., 2014; Meszner et al., 2011). However, during the LGM climatic conditions were cold and dryer, making extended pedogenic processes unlikely to occur. Consequently, the high a* values have a different origin. Since the nearby exposed sandstones of the Buntsandstein have a reddish color, they are most likely the cause for the high a* values. Moreover, the ice wedges seen in the field support the time frame of the LGM.

The lower part of *unit II* is also displaying hydromorphic conditions since the material is greyish and bleached. This interpretation is supported by a reduction of the redox potential (Mn/Fe), lower a* and b* values and a shift towards finer grain-size particles (e.g. Antoine et al., 2009; Antoine et al., 2001; Terhorst et al., 2001). Further, there is an increase of the mass specific magnetic susceptibility between *unit III.I* and *unit II.II*. Similar results have been found in Saxony (e.g. Baumgart et al., 2013; Lauer et al., 2014). They argue that this shift is due to sedimentation conditions and therefore use the mass specific magnetic susceptibility as an indicator to distinguish between laminated and homogenous Upper Weichselian Pleniglacial loess (see e.g. Baumgart et al., 2013; Lauer et al., 2014; Meszner et al., 2014; Meszner et al., 2011). The upper part of *unit II* covers the last strong phase of aeolian material input under relative cold and dry conditions, indicated by high values of GSI and U-ratio (Fig. 3B) but also by a relatively stable magnetic susceptibility. Ba/Sr, CPA, CIA and a* point towards slight weathering by elevated values within the upper first centimeters of *unit II*. This may be connected to the recent pedogenic processes above (Blume et al., 2010).

Unit I represents the recent soil. The high values of $CaCO_3$ at the bottom of *unit I* (*unit I.II*) are caused by a secondary $CaCO_3$ enrichment. Further, the clay content is elevated in *unit I.II,* suggesting that $CaCO_3$ and clay minerals were depleted in the upper part of *unit I* and enhanced at the bottom due to recent pedogenesis (Blume et al., 2010). On the other hand, the values of the weathering indices Rb/Sr, Ba/Sr, CIA and CPA are strongly reduced in *unit I.II*. This decrease can be interpreted as not only a result of reduced weathering but additionally the enrichment of clay minerals and $CaCO_3$. Since $CaCO_3$ is strongly influencing the behavior of other minerals, it is assumed to have a major contribution leading to the strong drop of the weathering indices here (Appendix 3; Buggle et al., 2011). The upper part is strongly weathered due to recent pedogenic processes displayed by all proxies (Blume et al., 2010). In comparison to the rest of the profile the mass specific and frequency dependent susceptibility are strongly enhanced, displaying the recent pedogenesis well. Several studies (e.g. Baumgart et al., 2013; Buggle et al., 2014; Gocke et al., 2014; Hošek et al., 2015) have shown the magnetic susceptibility to be a parameter which is influenced by a variety of processes in Western and Central Europe. Due to rather strong disturbances resulting from those surface processes an interpretation of the magnetic susceptibility features is challenging. An enhancement of the magnetic susceptibility due to pedogenesis is commonly only visible within recent soils. Signals of the deeper layers have to be interpreted with reservations, since alteration of ferromagnetic minerals may have resulted in the decreased magnetic susceptibility here (see e.g. Chen et al., 2015; Liu et al., 1999).

5.2. Zilly

As expected from field observations, the Zilly profile displays changes in environmental conditions, though the tundra gleys (bleached layers) are not consistently supported by the geochemical and color data (Fig. 8). In general, no proxy was found to constantly match the bleached horizons identified in the field. Therefore, a combination of proxies should be applied, to identify such horizons.

Similar to Hecklingen, there seems to be a shift in material source, based on an increased upper coarse silt and general sand content in *unit III* and the lower part of *unit II.IV* (Appendix 2; also visualized by the grain-size distribution heatmap in Appendix 5). The middle and coarse sand range is absent above (see Figs. 6B, 7). Sandy layers of Cretaceous age are exposed several kilometers north and east of the profile (see Fig. 2). These may have delivered source material for the sand input phase in Zilly. The depletion of mass specific susceptibility is similar to Hecklingen sediments of the LGM supporting the possible change in

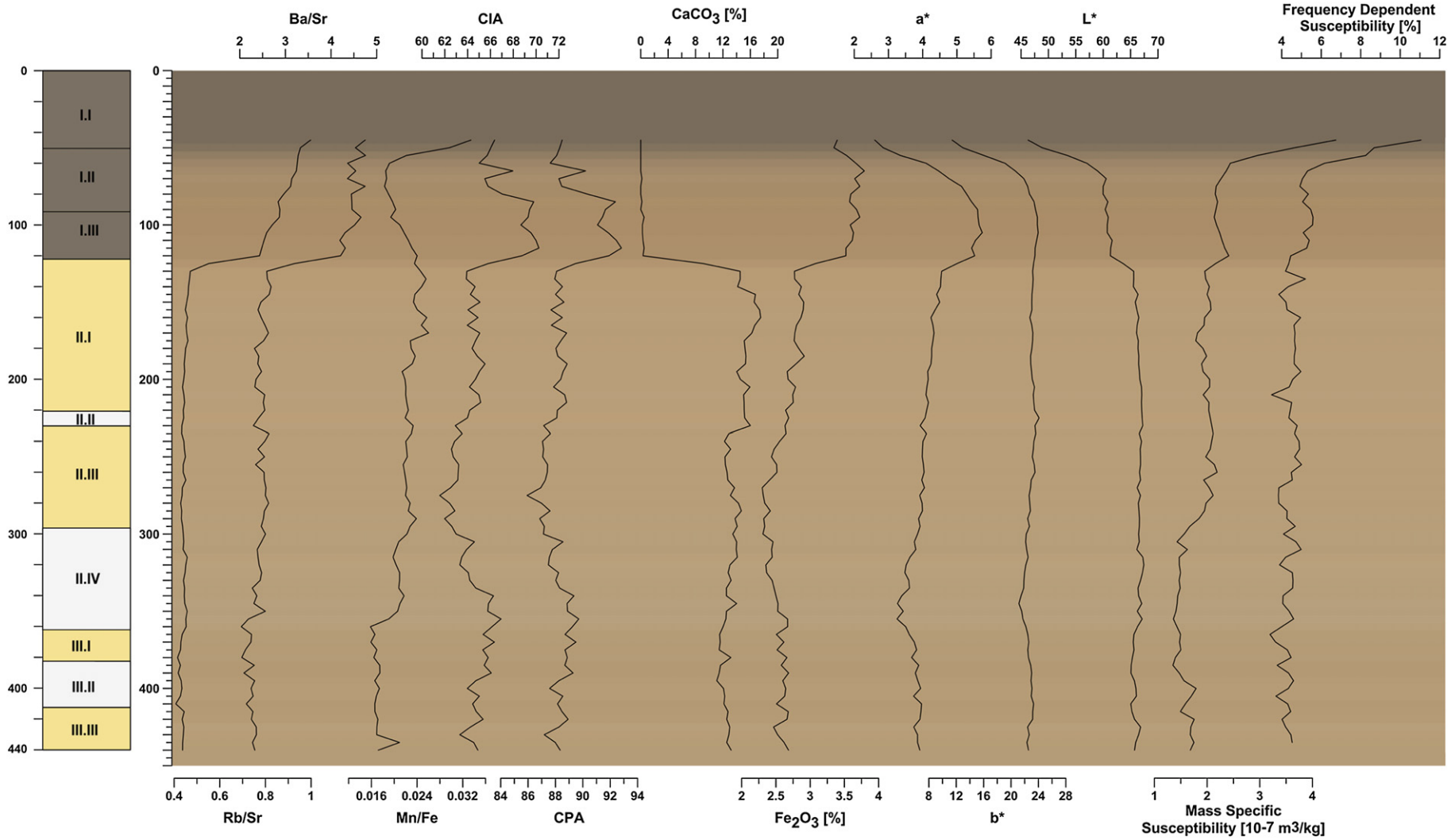

Fig. 8. Zilly (from left to right): Weathering indices, color data and magnetic susceptibility in relation to the simplified lithology based on defined units, plotted against depth [cm] (with color data plotted in the background).

source material. Consequently, *unit III* might represent a shift in wind direction towards stronger and more easterly winds, too. Further, the elevated GSI and U-ratio support the assumption of stronger aeolian dynamics (Fig. 6B). Thus, *unit III* appears to indicate the presence of LGM material within the Zilly profile. Due to missing ages below 2.44 m depth (see Table 1) this theory cannot be proven or dismissed, but in connection to the Hecklingen profile where similar features can be observed (lamination and slight cryoturbation of the material), the presence of the LGM is very possible.

Unit II.IV shows hydromorphic conditions since the material is greyish and bleached. The material above shows no lamination. The small increase of mass specific magnetic susceptibility indicates a change in sedimentation conditions similar to Hecklingen (see Chapter 5.1 *unit II.II*). In *unit II.III,* the elevated GSI and U-ratio indicate an increased wind dynamics. Relative dry conditions during the phase when *unit II.III* until *unit II.I* was accumulated are indicated by the low but relatively stable mass specific susceptibility.

Between *unit I* and *unit II* a strong shift occurs in most weathering proxies. Undoubtedly, the material below *unit I* has rarely experienced any weathering (Fig. 8) but due to the general influence of $CaCO_3$ on other elements, weathering proxies are most valuable in material lacking $CaCO_3$ (Buggle et al., 2011). The weathering of the recent soil material is displayed by the weathering indices well. Thus, the strong drop of weathering indices between *unit I* and *unit II* may be explained by the immediate increase of $CaCO_3$ at the bottom of *unit I* rather than through a truncation of the material below and redepositing of soil material above. The grain-size supports an interpretation of no (major) hiatus by the smooth decrease in clay towards *unit II*.

5.3. Summarizing the comparison of Hecklingen and Zilly with an outlook to other Western and Central European loess-paleosol sequences

Both investigated profiles have in common that they are rather strongly disturbed, especially by the permafrost related processes, such as cryoturbation (see Figs. 3A, 6A). Further, tundra gleys which can be clearly identified in the field were in general weakly developed and all were laterally traceable (see Figs. 3A, 6A). The weak development of the soils is likely the cause for the only small enhancements of clay content and slight increases of weathering proxies; it might also be responsible for the inconsistent signal of the tundra gleys. LPS further to the west and south-west in Europe show stronger enhancements of clay fraction and stronger geochemical weathering (e.g. Antoine et al., 2009; Vandenberghe et al., 1998). This could be caused by dryer and colder conditions compared to those regions, due to the vicinity of the Scandinavian ice sheet and the rain shadow of the Harz Mountains (see Fig. 1).

Features within the Hecklingen profile make it possible to link the sequence to other profiles in Western and Central Europe (see Fig. 9). Reinecke (2006) named the tundra gley (*unit VI.II)* at the bottom of the sequence (see Fig. 3A) "Hecklingen soil". Within the northern Harz foreland an equivalent was only found in one further profile situated close by (Ermsleben, see Reinecke, 2006). In the Nussloch section Löscher and Zöller (2001) and Antoine et al. (2001) described in one sub-profile a thin but similar layer ("Nussloch-Soil") below the Graselberg soil, dated to 65 ka and ~66.9 ± 5.1 ka. In Saxony, the only profile having gleyic material dated to 65 ka is the Rottewitz section (Meszner et al., 2014; Meszner et al., 2013). As mentioned above, other profiles in Saxony show an unconformity at that time and during the MIS 3. One reason for the preservation or even the development of the tundra gley in Hecklingen might be that the rain shadow of the Harz Mountains caused much dryer conditions than in other regions (Döring, 2004). In Western and Central Europe, this period is usually characterized by reworked Eemian and Early Weichselian soils or unconformities due to higher precipitations in combination with higher slope angles, causing e.g. slope wash processes (e.g. Rohdenburg and Meyer, 1966; Semmel, 1989; Meszner et al., 2013).

According to Reinecke's (2006) age for the soil material (whole *unit V*), the material appears to be from an earlier stage of MIS 3. Here it is suggested that the material is an equivalent to the Graselberg soil (see Fig. 9; e.g. Antoine et al., 2001; Gocke et al., 2014). The data lead to the assumption that during an earlier phase of the MIS 3 the environmental conditions in Hecklingen were more stable than in other regions of the northern European loess belt (e.g. Meszner et al., 2013; Schirmer, 2016). This is indicated by the smooth transition from *unit VI.I* (loess) towards *unit V.II* (truncated soil layer) by all proxies and by the existence of crotovinas in the truncated soil layer. There had to be a stable phase present during which macro fauna was able to cause those large burrows. Further, the preservation of accumulated soil material above (*unit V.I*) and the probable pedogenic overprinting (accumulated soil material experienced a further pedogenesis) does indicate an additional stable phase. The rain shadow of the Harz Mountains might have played a large role in preserving the MIS 3 soil material here as well. Assuming similar precipitation gradients as today, reduced precipitation resulted in less intrusive erosional events than in other regions. However, the stone layer *unit IV.V* marks a strong erosion phase during late MIS 3 and/or early MIS 2, as mentioned before.

Following the nomenclature of Schönhals et al. (1964) with further advances by Bibus (2002), the soils E1 and E0 appear to be missing. The two horizons which are usually found in the E2 soil might be the analogue to the layers *unit IV.II* and *IV.IV*, and the *unit III.II* tundra gley could be related to the weakly developed E3.

In the area of the Lower Rhine Embayment and adjacent areas the transition between the LGM and the last cover loess is marked by an immediate change of sediment characteristics. The material changes from being cryoturbated and laminated during the LGM, towards homogeneous aeolian sediments of the last cover loess (e.g. Haesaerts, 1985; Kels, 2007; Schirmer, 2003a). The initiation of the new phase (last cover loess) is marked by a tundra gley which is supported by a shift in grain-size towards finer material predominantly. The nomenclature of Schönhals et al. (1964) with further advances by Bibus (2002) defines that tundra gley as E4 soil (Zens et al., 2016). Taking the findings of Schmidt et al. (2011) and Frechen and Schirmer (2011) concerning the fading rates and the resulting ages of the material into account, an equivalent to the E4 is present in Hecklingen (see *unit II.II*) and marks transition from LGM (*unit III.I*) to last cover loess (*II.I*), supporting prior assumptions.

Based on the very likely shift in source material in both profiles, Hecklingen and Zilly can be linked to each other (see Fig. 9). Despite the fact that Hecklingen and Zilly cover a different time resolution and have different source materials, the parallelization of the sequences mainly based on changes in grain-size distribution indicates the presence of material from the time of the last cover loess and the LGM which further suggests that both sequences experienced similar environmental conditions and surface processes during that time frame (see Figs. 3B, 6B).

6. Conclusion

Our study with a high resolution multi-proxy approach used for two loess-paleosol-sequences from the northern Harz foreland (Germany) gives new insights about the environmental and climatic conditions during the last glacial in an area close to the Scandinavian ice sheet. The main findings are:

- In both profiles sediments of the LGM and last cover loess period are present.
- Hecklingen and Zilly experienced an increased input of aeolian material during the last cover loess period, supporting the theory of dryer and colder conditions for this time frame.
- The same is valid for the LGM. Additionally, the considerably enhanced short distance input within the LGM sediments points towards a shift in wind regime with a higher frequency of strong

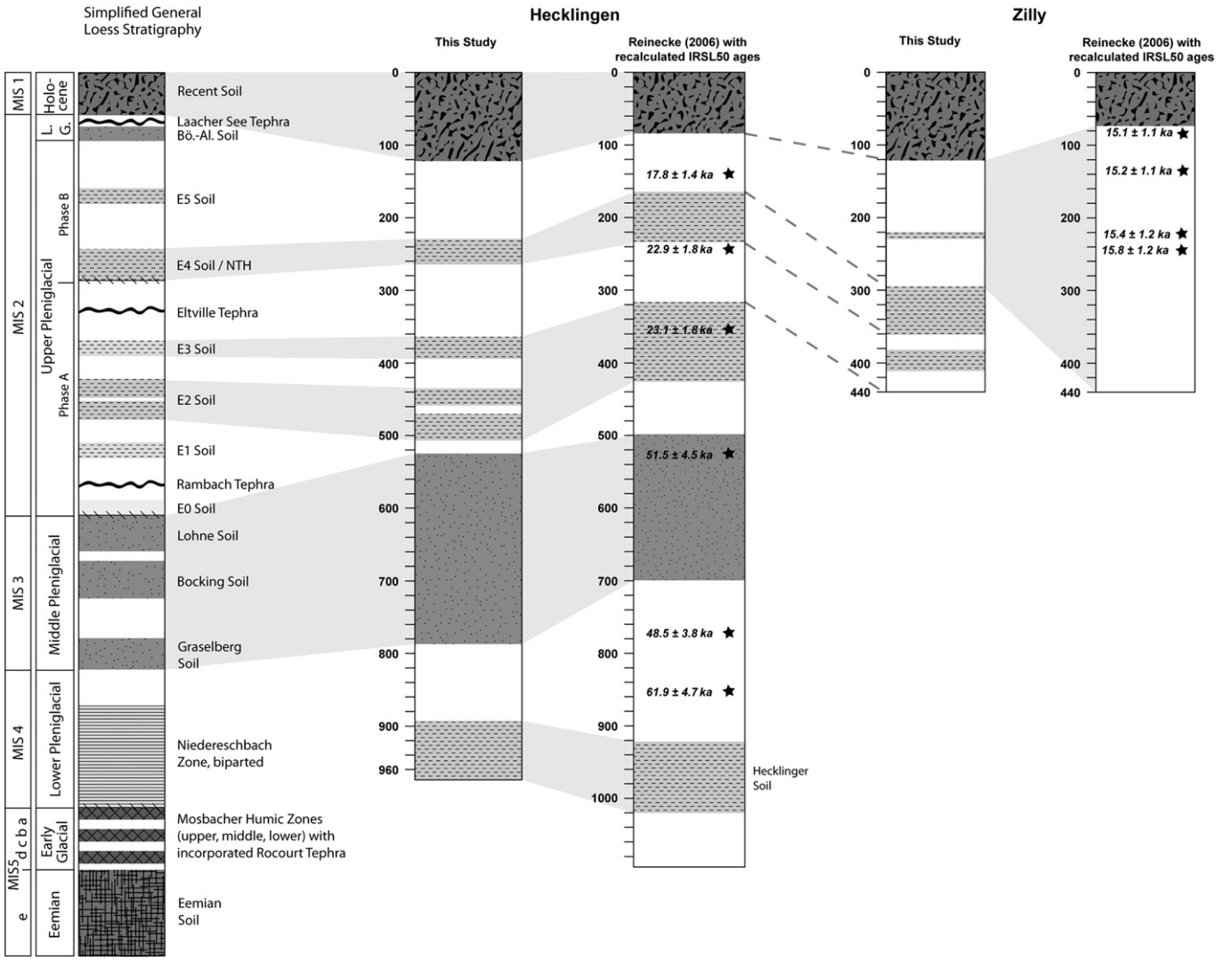

Fig. 9. Correlation of the recent findings in Hecklingen and Zilly to Reinecke's (2006) findings including recalculated IRSL50 ages, and to a generalized stratigraphy of Central Europe (after Zens et al. (2016) modified after Schönhals et al. (1964) and Bibus (2002)). Reinecke (2006) defined the here as one soil complex visualized MIS 3 soil complex as followed: lower 50 cm are reworked soil sediments flowed by 70 cm of in-situ soil. Above that soil follows 60 cm of reworked soil sediment with no post-depositional signs of soil formation. The MIS 3 soil complex of the recent study is also summarized as one complex, here. The structure is as follows: the lower 70 cm are defined as truncated in-situ soil material (unit V.II) followed by 1.9 m of reworked soil sediment with signs of post-depositional pedogenic overprinting (unit V.I).

easterly wind conditions with several dust storm events.

- In Hecklingen, elevated values of coarser material within MIS 3 soil was observed, too, which speaks for the occurrence of erosion and re-deposition processes of soil material with signs of post-depositional pedogenic overprinting during the MIS 3.
- The presence of MIS 3 soil material itself allows the conclusion that surface processes were less intrusive at least partially during the MIS 3 and the MIS 2 in the northern Harz foreland than in other Western and Central European regions e.g. wide parts of the Lower Rhine Embayment and Saxony.

Hecklingen in particular seems to represent the changes of environmental conditions during large parts of the Weichselian well. It will be beneficial for a better understanding of environmental conditions during the Weichselian to use additional proxies and dating methods at these profiles but also adding new locations for a larger scale approach.

Acknowledgements

This project is affiliated to the CRC 806 "Our way to Europe", subproject D1 "Analysis of Migration Processes due to Environmental Conditions between 40,000 and 14,000 a BP in the Rhine-Meuse Area". We thank the German Science Foundation (DFG, grant number INST 216/602-2) for funding this project. We thank Marianne Dohms for her help with laboratory analysis, Janek Walk for generating the geological map, and the OSL-Lab of the University of Cologne for providing the OSL-Results. Further, we thank Ulrich Hambach for support concerning the magnetic susceptibility data evaluation.

Appendix A. Supplementary data

Supplementary data to this article can be found online at http://dx.doi.org/10.1016/j.palaeo.2016.09.001.

References

Allen, J.R.L., Thornley, D.M., 2004. Laser granulometry of Holocene estuarine silts: effects of hydrogen peroxide treatment. The Holocene 14 (2), 290–295. http://dx.doi.org/10.1191/0959683604hl681rr.

Altermann, M., Fiedler, H.-J., 1975. Substrat- und Bodenwechsel am nördlichen Lößrand des Schwarzerdengebietes der DDR. Hercynia N.F. 12 (2), 130–159.

Antoine, P., Rousseau, D.-D., Zöller, L., Lang, A., Munaut, A.-V., Hatté, C., Fontugne, M., 2001. High-resolution record of the last Interglacial–glacial cycle in the Nussloch loess–palaeosol sequences, Upper Rhine Area, Germany. QI 76–77, 211–229. http://dx.doi.org/10.1016/S1040-6182(00)00104-X.

Antoine, P., Rousseau, D.-D., Moine, O., Kunesch, S., Hatté, C., Lang, A., Tissoux, H., Zöller, L., 2009. Rapid and cyclic aeolian deposition during the Last Glacial in European loess: a high-resolution record from Nussloch, Germany. QSR 28 (25–26), 2955–2973. http://dx.doi.org/10.1016/j.quascirev.2009.08.001.

Assallay, A.M., Rogers, C.D.F., Smalley, I.J., Jefferson, I.F., 1998. Silt: 2–62 mm, 9–4φ. Earth-Science Reviews 45, 61–88.

Baumgart, P., Hambach, U., Meszner, S., Faust, D., 2013. An environmental magnetic fingerprint of periglacial loess: Records of Late Pleistocene loess–palaeosol sequences from Eastern Germany. QI 296, 82–93. http://dx.doi.org/10.1016/j.quaint.2012.12.021.

Bibus, E., 2002. Zum Quartär im mittleren Neckarraum: Reliefentwicklung, Löß/Paläobodensequenzen, Paläoklima Tübinger Geogr. Arb. 8 Geogr. Dept. University Tübingen.

Billwitz, K., Haase, G., 1964. Das sächsische Lößhügelland zwischen Mulde und Elbe und seine nördlichen Randgebiete. Exkursionsführer der 7. Wiss. Hauptverslg. Geogr. Ges. der DDR, pp. 81–95.

Blott, S.J., Pye, K., 2012. Particle size scales and classification of sediment types based on size distributions: review and recommended procedures. Sedimentology 59 (7), 2071–2096. http://dx.doi.org/10.1111/j.1365-3091.2012.01335.x.

Blume, H.-P., Brümmer, G.W., Horn, R., Kandeler, E., Kögel-Knabner, I., Kretzschmar, R., Stahr, K., Wilke, B.-M., 2010. Scheffer/Schachtschabel - Lehrbuch der Bodenkunde. 16th edition. completely revised.

Boenigk, W., Frechen, M., 2001. The loess record in sections at Koblenz–Metternich and Tönchesberg in the Middle Rhine Area. QI 76–77, 201–209. http://dx.doi.org/10.1016/S1040-6182(00)00103-8.

Bork, H.R., Rohdenburg, H., 1979. Beispiele für jungholozäne Bodenerosion und Bodenbildung im Untereichsfeld und seinen Randgebieten. Landschaftsgenese und Landschaftsökologie 3, 115–134.

Brennan, B.J., 2003. Beta doses to spherical grains. Radiat. Meas. 37, 299–303.

Brosche, K.-U., Walther, M., 1978. Die jungpleistozänen Deckschichten der Braunkohletagebaue der Braunschweigischen Kohlebergwerke (BKB) zwischen Helmstedt und Schöningen. E&G – Quaternary Science Journal 28, 51–67.

Brosche, K.-U., Walther, M., 1991. Untersuchungen zur Lößstratigraphie und jungpleistozänen Formung in Südniedersachsen und östlichen Westfalen. Geographica-Oekologica 2, 1–52.

Brunnacker, K., 1967. Fundamentals of Quaternary soil stratigraphy in southern Germany. In: Morrison, R.B., Wright, H.R. (Eds.), Quaternary Soils. Proceedings of the 7th INQUA Congress 9, pp. 93–102.

Buggle, B., Glaser, B., Hambach, U., Gerasimenko, N., Marković, S., 2011. An evaluation of geochemical weathering indices in loess–paleosol studies. QI 240 (1–2), 12–21. http://dx.doi.org/10.1016/j.quaint.2010.07.019.

Buggle, B., Hambach, U., Müller, K., Zöller, L., Marković, S.B., Glaser, B., 2014. Iron mineralogical proxies and Quaternary climate change in SE-European loess–paleosol sequences. Catena 117, 4–22. http://dx.doi.org/10.1016/j.catena.2013.06.012.

Bundesanstalt für Geowissenschaften und Rohstoffe (BGR), 2015. General Geological Map of Germany 1:200,000 (GUEK200) (Hannover).

Chen, J., Liu, X., Kravchinsky, V.A., Lü, B., Chen, Q., 2015. Post-depositional forcing of magnetic susceptibility variations at Kurtak section, Siberia. QI http://dx.doi.org/10.1016/j.quaint.2015.09.092 (in press).

Clark, P.U., Dyke, A.S., Shakun, J.D., Carlson, A.E., Clark, J., Wohlfarth, B., Mitrovica, J.X., Hostetler, S.W., McCabe, A.M., 2009. The Last Glacial Maximum. Science 325 (5941), 710–714. http://dx.doi.org/10.1126/science.1172873.

Cullers, R.L., 2000. The geochemistry of shales, siltstones and sandstones of Pennsylvanian–Permian age, Colorado, USA: implications for provenance and metamorphic studies. Lithos 51 (3), 181–203. http://dx.doi.org/10.1016/S0024-4937(99)00063-8.

Dietrich, S., Seelos, K., 2010. The reconstruction of easterly wind directions for the Eifel region (Central Europe) during the period 40.3–12.9 ka BP. Clim. Past 6 (2), 145–154.

Döring, J., 2004. Zu den Klimaverhältnissen im östlichen Harzvorland. Hercynia N.F. 37 (2), 137–154.

Durcan, J.A., King, G.E., Duller, G.A.T., 2015. DRAC: Dose Rate and Age Calculator for trapped charge dating. Quat. Geochronol. 28, 54–61. http://dx.doi.org/10.1016/j.quageo.2015.03.012.

Eckmeier, E., Egli, M., Schmidt, M.W.I., Schlumpf, N., Nötzli, M., Minikus-Stary, N., Hagedorn, F., 2010. Preservation of fire-derived carbon compounds and sorptive stabilisation promote the accumulation of organic matter in black soils of the Southern Alps. Geoderma 159 (1–2), 147–155. http://dx.doi.org/10.1016/j.geoderma.2010.07.006.

Ehlers, J., Eissmann, L., Lippstreu, L., Stephan, H.-J., Wansa, S., 2004. Pleistocene glaciation of North Germany. In: Ehlers, J., Gibbard, P.L. (Eds.), Quaternary Glaciation – Extent and Chronology, Part I: Europe. Developments in Quaternary Sciences 2, pp. 135–146.

Ehlers, J., Grube, A., Stephan, H.J., Wansa, S., 2011. Pleistocene glaciation of North Germany – New results. In: Ehlers, J., Gibbard, P.L., Hughes, P.D. (Eds.), Quaternary Glaciation – Extent and Chronology. A Closer Look. Developments in Quaternary Sciences 15, pp. 149–162.

Fabig, I., 2007. Die Niederschlags- und Starkregenentwicklung der letzten 100 Jahre im Mitteldeutschen Trockengebiet als Indikatoren möglicher Klimaänderungen (Diss.) Martin-Luther-University Halle-Wittenberg.

Feldmann, L., 2002. Das Quartär zwischen Harz und Allertal – mit einem Beitrag zur Landschaftsgeschichte im Tertiär. Clausthal University, Habil.

Fischer, P., 2010. Zur mittel- und jungquartären Relief- und Bodenentwicklung der nordwestlichen Kölner Bucht - Detailuntersuchungen der lössbedeckten Mittelterrassenlandschaft (Diss.) Cologne University.

Fischer, P., Hilgers, A., Protze, J., Kels, H., Lehmkuhl, F., Gerlach, R., 2012. Formation and geochronology of Last Interglacial to Lower Weichselian loess/palaeosol sequences – case studies from the Lower Rhine Embayment, Germany. E&G - Quaternary Science Journal 61, 48–63.

Fitzsimmons, K.E., Marković, S.B., Hambach, U., 2012. Pleistocene environmental dynamics recorded in the loess of the middle and lower Danube basin. QSR 41, 104–118. http://dx.doi.org/10.1016/j.quascirev.2012.03.002.

Frechen, M., Schirmer, W., 2011. Luminescence Chronology of the Schwalbenberg II Loess in the Middle Rhine Valley. Quaternary Science Journal 60, 78–89. http://dx.doi.org/10.3285/eg.60.1.05.

Frechen, M., Schweitzer, U., Zander, A., 1996. Improvements in sample preparation for the fine grain technique. Ancient TL 14, 15–17.

Frechen, M., Zander, A., Cílek, V., Ložek, V., 1999. Loess chronology of the Last Interglacial/Glacial cycle in Bohemia and Moravia, Czech Republic. QSR 18 (13), 1467–1493. http://dx.doi.org/10.1016/S0277-3791(98)00087-0.

Frechen, M., Oches, E.A., Kohfeld, K.E., 2003. Loess in Europe—mass accumulation rates during the Last Glacial Period. QSR 22 (18–19), 1835–1857.

Galbraith, R.F., Roberts, R.G., Laslett, G.M., Yoshida, H., Olley, J.M., 1999. Optical dating of single grains of quartz from Jinmium rock shelter, northern Australia. Part I: experimental design and statistical models. Archaeometry 41, 339–364.

Gehrt, E., 1994. Die äolischen Sedimente im Bereich der nördlichen Lössgrenze zwischen Leine und Oker und deren Einflüsse auf die Bodenentwicklung (Diss.) Göttingen University.

Gehrt, E., Hagedorn, J., 1996. Zur Entstehung der nördlichen Lössgrenze in Mitteleuropa. Landesamt f. Natur u. Umwelt S.-H. Abt. Geologie/Boden. Festschrift Prof. Dr. Stremme, pp. 59–66.

Göbeler, W., 1966. Die Entwicklung der äolischen Decken und der Böden im Bereich der nördlichen Lößgrenze. Wiss. Zeitschrift Karl-Marx-Univ. Leipzig. Math.-Nat. Reihe 15 (4), 713–720.

Gocke, M., Hambach, U., Eckmeier, E., Schwark, L., Zöller, L., Fuchs, M., Löscher, M., Wiesenberg, G.L.B., 2014. Introducing an improved multi-proxy approach for paleoenvironmental reconstruction of loess–paleosol archives applied on the Late Pleistocene Nussloch sequence (SW Germany). Palaeogeogr. Palaeoclimatol. Palaeoecol. 410, 300–315. http://dx.doi.org/10.1016/j.palaeo.2014.06.006.

Guérin, G., Mercier, N., Adamiec, G., 2011. Dose-rate conversion factors: update. Ancient TL 29 (1), 5–8.

Haase, G., Lieberoth, I., Ruske, R., 1970. Sedimente und Paläoböden im Lößgebiet. In: Richter, H., Haase, G., Lieberoth, I., Ruske, R. (Eds.), Periglazial – Löß – Paläolithikum im Jungpleistozän der Deutschen Demokratischen Republik 274. Petermanns Geographischen Mitteilungen, pp. 99–212.

Haase, D., Fink, J., Haase, G., Ruske, R., Pécsi, M., Richter, H., Altermann, M., Jäger, K.-D., 2007. Loess in Europe – its spatial distribution based on a European Loess Map, scale 1:2,500,000. QSR 26, 1301–1312.

Haesaerts, P., 1985. Les loess du Pléistocène supérieur en Belgique. Comparaisons avec les séquences d'Europe centrale. Bulletin de l'Association française pour l'étude du quaternaire 22 (2–3), 105–115. http://dx.doi.org/10.3406/quate.1985.1534.

Haesaerts, P., Juvigné, E., Kuyl, O., Mucher, H., Roebroeks, W., 1981. Compte rendu de l'excursion du 13 juin 1981, en Hesbaye et au Limbourg Néerlandais, consacrée à la chronostratigraphie des loess du Pléistocène supérieur. Annales Société Géologique Belgique 104, 223–240.

Haesearts, P., Pirson, S., Meijs, E., 2011. New proposal for the Quaternary lithostratigraphic units (Belgium). Submission Quaternary, Proposal and discussions.

Hilgers, A., Gehrt, E., Janotta, A., Radtke, U., 2001. A contribution to the dating of the northern boundary of the Weichselian Loess Belt in Northern Germany by luminescence dating and pedological analysis. QI 76–77, 191–200. http://dx.doi.org/10.1016/S1040-6182(00)00102-6.

Hošek, J., Hambach, U., Lisá, L., Grygar, T.M., Horáček, I., Meszner, S., Knésl, I., 2015. An integrated rock-magnetic and geochemical approach to loess/paleosol sequences from Bohemia and Moravia (Czech Republic): implications for the Upper Pleistocene paleoenvironment in central Europe. Palaeo 3 (418), 344–358. http://dx.doi.org/10.1016/j.palaeo.2014.11.024.

Huntley, D.J., Baril, M.R., 1997. The K content of the K-feldspars being measured in optical dating or in thermoluminescence dating. Ancient TL 15, 11–12.

ISO 11277 (2002): Soil quality - determination of particle size distribution in mineral soil material - method by sieving and sedimentation (ISO 11277:1998 + ISO 11277:1998 Corrigendum 1:2002).

ISO, B. 13320-1 (1999): Particle size analysis-Laser diffraction methods.

ISO, E. 14688 (2002): Geotechnical investigation and testing. Identification and classification of soil.

ISO, N. 10693 (1995): Soil quality–determination of carbonate content–volumetric method.

Kehl, M., Eckmeier, E., Franz, S.O., Lehmkuhl, F., Soler, J., Soler, N., Reicherter, K., Weniger, G.C., 2014. Sediment sequence and site formation processes at the Arbreda Cave, NE Iberian Peninsula, and implications on human occupation and climate change during the Last Glacial. Clim. Past. 10, pp. 1673–1692. http://dx.doi.org/10.5194/cp-10-1673-2014.

Kels, H., 2007. Bau und Bilanzierung der Lössdecke am westlichen Niederrhein (Diss) Heinrich-Heine-University Düsseldorf.

Kels, H., Schirmer, W., 2010. Relation of loess units and prehistoric find density in the Garzweiler open-cast mine, Lower-Rhine. E&G – Quaternary Science Journal 59 (1–2), 59–65.
Krauß, L., Schmidt, G., Zierdt, M., Frühauf, M., 2013. Experimentelle Bestimmung präferenzieller Fließpfade infiltrierten Niederschlags am Beispiel einer Schwarzerde und einer Pararendzina der Querfurter Platte. Hercynia N.F. 46, 21–40.
Kreutzer, S., Fuchs, M., Meszner, S., Faust, D., 2012. OSL chronostratigraphy of a loess-palaeosol sequence in Saxony/Germany using quartz of different grain sizes. Quat. Geochronol. 10, 102–109. http://dx.doi.org/10.1016/j.quageo.2012.01.004.
Kreutzer, S., Lauer, T., Meszner, S., Krbetschek, M.R., Faust, D., Fuchs, M., 2014. Chronology of the Quaternary profile Zeuchfeld in Saxony-Anhalt / Germany – a preliminary luminescence dating study. Z. Geomorphol. 58 (1), 5–26. http://dx.doi.org/10.1127/0372-8854/2012/S-00112.
Kunert, R., Altermann, M., 1965. Das Pleistozän zwischen Saale und Wipper. Geologie 14, 520–552.
Landesamt für Geologie und Bergwesen Sachsen-Anhalt (LAGB) [eds.] (2006): Bodenbericht Sachsen-Anhalt 2006. Böden und Bodeninformationen in Sachsen-Anhalt. Mitteilungen zu Geologie und Bergwesen in Sachsen-Anhalt 11.
Lauer, T., Von Suchodoletz, H., Vollmann, H., Meszner, S., Frechen, M., Tinapp, C., Goldmann, L., Müller, S., Zielhofer, C., 2014. Landscape aridification in Central Germany during the late Weichselian Pleniglacial results from the Zauschwitz loess site in western Saxony. Zeitsch. f. Geomorph. 58 (Suppl. 1), 27–50. http://dx.doi.org/10.1127/0372-8854/2013/S-00163.
Lehmkuhl, F., Zens, J., Krauß, L., Schulte, P., Kels, H., 2016. Loess-paleosol sequences at the Northern European Loess Belt in Germany: distribution, geomorphology and stratigraphy. QSR (in review).
Litt, T., Wansa, S., 2008. In: Bachmann, G.H., Ehling, B.-C., Eichner, R., Schwab, M. (Eds.), Quartär. Geologie von Sachsen-Anhalt, Stuttgart.
Liu, X.M., Hesse, P., Rolph, T., Begét, J.E., 1999. Properties of magnetic mineralogy of Alaskan loess: evidence for pedogenesis. QI 62 (1), 93–102. http://dx.doi.org/10.1016/S1040-6182(99)00027-0.
Löscher, M., Zöller, L., 2001. Lössforschung im nordwestlichen Kraichgau.- Jber. Mitt. oberrhein. Geol. Ver., N.F. 83, 317–326.
Ludwig, P., Schaffernicht, E.J., Shao, Y., Pinto, J.G., 2016. Regional atmospheric circulation over Europe during the Last Glacial Maximum and its links to precipitation. J. Geophys. Res. Atmos. 121, 2130–2145. http://dx.doi.org/10.1002/2015JD024444.
Mania, D., 2003. Die Molluskenfauna der mittel- und jungpleistozänen Abfolge von Lengefeld bei Bad Kösen im Saaletal und ihre Aussage für Klimaentwicklung und Stratigraphie. Praehistoria Thuringica 9, 117–162.
Mania, D., Altermann, M., 2001. Die Deckschichtenfolge von Lengefeld bei Bad Kösen im mittleren Saaletal – ein Typusprofil für die Quartärstratigraphie. Praehistoria Thuringica 6/7, 103–131.
Marković, S.B., Hambach, U., Stevens, T., Kukla, G.J., Heller, F., McCoy, W.D., Oches, E.A., Buggle, B., Zöller, L., 2011. The last million years recorded at the Stari Slankamen (Northern Serbia) loess-palaeosol sequence: revised chronostratigraphy and long-term environmental trends. QSR 30 (9–10), 1142–1154. http://dx.doi.org/10.1016/j.quascirev.2011.02.004.
McLennan, S.M., 1993. Weathering and global denudation. Journal of Geology 101, 295–303.
Merkt, J., 1968. Erläuterung zur Karte der Lößverbreitung in Südniedersachsen. Geol. Jb. Hannover 86, 107–112.
Meszner, S., Fuchs, M., Faust, D., 2011. Loess-Palaeosol-Sequences from the loess area of Saxony (Germany). E&G – Quaternary Science Journal 60 (1), 47–65.
Meszner, S., Kreutzer, S., Fuchs, M., Faust, D., 2013. Late Pleistocene landscape dynamics in Saxony, Germany: Paleoenvironmental reconstruction using loess-paleosol sequences. QI 296, 94–107. http://dx.doi.org/10.1016/j.quaint.2012.12.040.
Meszner, S., Kreutzer, S., Fuchs, M., Faust, D., 2014. Identifying depositional and pedogenetic controls of Late Pleistocene loess-paleosol sequences (Saxony, Germany) by combined grain size and microscopic analyses. Z. Geomorphol. 58 (Suppl. 3), 063–090. http://dx.doi.org/10.1127/0372-8854/2014/S-00169.
Muhs, D.R., 2007. Loess deposits, origins and properties. In: Elias, S.A. (Ed.), Encyclopedia of Quaternary Science. Oxford, pp. 1405–1418 http://dx.doi.org/10.1016/B0-44-452747-8/00158-7.
Murray, A.S., Wintle, A.G., 2000. Luminescence dating of quartz using an improved single-aliquot regenerative-dose protocol. Radiat. Meas. 32, 57–73. http://dx.doi.org/10.1016/S1350-4487(99)00253-X.
Nesbitt, H.W., Young, G.M., 1982. Early Proterozoic climates and plate motions inferred from major element chemistry of lutites. Nature 299 (5885), 715–717.
Neumeister, H., 1966. Die Bedeutung äolischer Prozesse für die Eigenschaften periglazialer Hangsedimente im Ostthüringer Schiefergebirge. Wiss. Zeitschrift Karl-Marx-Univ. Leipzig. Math.-Nat. Reihe 15, 721–727.
Neumeister, H., 1971. Jungpleistozäne Decksedimente und Bodenentwicklung in der Umgebung von Leipzig. Zprávy Geografického Ústavu 8/6, 23–72.
Özer, M., Orhan, M., Işik, N.S., 2010. Effect of particle optical properties on size distribution of soils obtained by laser diffraction. Environmental & Engineering Geoscience 16 (2), 163–173. http://dx.doi.org/10.2113/gseegeosci.16.2.163.
Paas, W., 1968. Gliederung und Altersstellung der Lösse am Niederrhein. Fortschr. Geol. Rhld. u. Westf. 16, 185–196.
Patzelt, G., 2003. Nördliches Harzvorland (subhercyn), östlicher Teil. Sammlung geologischer Führer 96. Nordhausen.
Pécsi, M., 1990. Loess is not just the accumulation of dust. QI 7, 1–21. http://dx.doi.org/10.1016/1040-6182(90)90034-2.
Pécsi, M., Richter, G., 1996. Löss. Herkunft–Gliederung–Landschaften. Zeitschrift für Geomorphologie, N.F. Suppl. 98, Berlin, Stuttgart.
Poser, H., 1951. Die nördliche Lößgrenze in Mitteleuropa und das spätglaziale Klima. E&G – Quaternary Science Journal 1.
Prescott, J.R., Hutton, J.T., 1994. Cosmic ray contributions to dose rates for luminescence and ESR dating: Large depths and long-term time variations. Radiat. Meas. 23, 497–500. http://dx.doi.org/10.1016/1350-4487(94)90086-8.
Preusser, F., Andersen, B.G., Denton, G.H., Schlüchter, C., 2005. Luminescence chronology of Late Pleistocene glacial deposits in North Westland, New Zealand. QSR 24 (20−21), 2207–2227.
Pye, K., 1987. Aeolian Dust and Dust Deposits. Academic Press Inc., London, Orlando, San Diego, New York, Austin, Boston, Sydney, Tokyo, Toronto.
Pye, K., 1996. The nature, origin and accumulation of loess. QSR 14, 653–667.
Pye, K., Blott, S.J., 2004. Particle size analysis of sediments, soils and related particulate materials for forensic purposes using laser granulometry. Forensic Sci. Int. 144 (1), 19–27. http://dx.doi.org/10.1016/j.forsciint.2004.02.028.
Razinksi, K.-H., Beutler, G., Franzke, H.J., Ehling, B.-C., 2008. Nördliches Harzvorland (Subhercyn). In: Bachmann, G.H., Ehling, B.-C., Eichner, R., Schwab, M. (Eds.), Geologie von Sachsen-Anhalt Stuttgart.
Reinecke, V., 2006. Untersuchungen zur mittel- und jungpleistozänen Reliefentwicklung und Morphodynamik im nördlichen Harzvorland. Aachener Geographische Arbeiten 43.
Remy, H., 1960. Der Löß am unteren Mittel- und Niederrhein. E&G – Quaternary Science Journal 11, 107–120.
Renssen, H., Kasse, C., Vandenberghe, J., Lorenz, S.J., 2007. Weichselian Late Pleniglacial surface winds over northwest and central Europe: a model–data comparison. JQS 22, 281–293. http://dx.doi.org/10.1002/jqs.1038.
Ricken, W., 1983. Mittel- und jungpleistozäne Lößdecken im südwestlichen Harzvorland. Catena Suppl. 3, 95–138.
Rohdenburg, H., Meyer, B., 1966. Zur Feinstratigraphie und Paläopedologie des Jungpleistozäns nach Untersuchungen an südniedersächsischen und nordhessischen Lößprofilen. Mitt. Dtsch. Bodenkdl. Gesellsch. 5, 1–135.
Römer, W., Lehmkuhl, F., Sirocko, F., 2016. Late Pleistocene Aeolian Dust Provenances and Wind Direction Changes Reconstructed by Heavy Mineral Analysis of the Sediments of the Dehner Dry Maar (Eifel Mountains, Germany) (in review).
Rousseau, D.D., Antoine, P., Hatté, C., Lang, A., Zöller, L., Fontugne, M., Ben Othman, D., Luck, J.M., Moine, O., Labonne, M., Bentaleb, I., Jolly, D., 2002. Abrupt millennial climatic changes from Nussloch (Germany) Upper Weichselian eolian records during the Last Glaciation. QSR 21 (14–15), 1577–1582. http://dx.doi.org/10.1016/S0277-3791(02)00034-3.
Rousseau, D.-D., Sima, A., Antoine, P., Hatté, C., Lang, A., Zöller, L., 2007. Link between European and North Atlantic abrupt climate changes over the last glaciation. Geophys. Res. Lett. 34, L22713. http://dx.doi.org/10.1029/2007GL031716.
Ruske, R., Wünsche, M., 1961. Löß und fossile Böden im mittleren Saale- und unteren Unstruttal. Geologie 10, 9–29.
Ruske, R., Wünsche, M., 1964. Zur Gliederung des Pleistozäns im Raum der unteren Unstrut. Geologie 13 (2), 211–222.
Ruske, R., Wünsche, M., 1968. Zur Gliederung jungpleistozäner Lößablagerungen im südöstlichen und östlichen Harzvorland. Geologie 17, 288–297.
Ruske, R., Schulz, W., Wünsche, M., 1962. Pleistozäne Ablagerungen im Gebiet zwischen Leipzig und der unteren Unstrut unter besonderer Berücksichtigung der Lösse und fossilen Böden. Exkursionsführer Herbsttagung 1962 der Geol. Gesellschaft der DDR.
Schaller, K., 2000. Praktikum zur Bodenkunde und Pflanzenernährung. Geisenheimer Berichte 2. 8th edition. Geisenheim.
Schatz, A.-K., Scholten, T., Kühn, P., 2015. Paleoclimate and weathering of the Tokaj (Hungary) loess–paleosol sequence. Palaeogeogr. Palaeoclimatol. Palaeoecol. 426, 170–182. http://dx.doi.org/10.1016/j.palaeo.2015.03.016.
Schirmer, W., 2000. Eine Klimakurve des Oberpleistozäns aus dem rheinischen Löss. E&G – Quaternary Science Journal 50, 25–49.
Schirmer, W., 2003a. Die Eben-Zone im Oberwürmlöss zwischen Maas und Rhein. In: Schirmer, W. (Ed.), Landschaftsgeschichte im Europäischen Rheinland 4. GeoArchaeoRhein, pp. 351–416.
Schirmer, W., 2016. Late Pleistocene loess of the Lower Rhine. QI http://dx.doi.org/10.1016/j.quaint.2016.01.034 (in press).
Schmidt, R., 1971. Die Weichselzeit im Übergangsbereich zwischen Löss und Treibsand in Nordsachsen (Grossheiner Gebiet). Zprávy Geografického Ústavu 8/6, 1–23.
Schmidt, E.D., Semmel, A., Frechen, M., 2011. Luminescence dating of the loess/palaeosol sequence at the gravel quarry Gaul/Weilbach, Southern Hesse (Germany). Quaternary Science Journal 60, 116–125. http://dx.doi.org/10.3285/eg.60.1.08.
Schönhals, E., Rohdenburg, H., Semmel, A., 1964. Ergebnisse neuerer Untersuchungen zur Würmlöß-Gliederung in Hessen. E&G – Quaternary Science Journal 15, 199–206.
Schulte, P., Lehmkuhl, F., 2016. The difference of two laser diffraction patterns as an indicator for post-depositional grain size reduction in loess-paleosol sequences. Geophysical Research: Earth Surface (in review).
Schulte, P., Lehmkuhl, F., Steininger, F., Loibl, D., Lockot, G., Protze, J., Fischer, P., Stauch, G., 2016. Influence of HCl pretreatment and organo-mineral complexes on laser diffraction measurement of loess-paleosol-sequences. Catena 137, 392–405. http://dx.doi.org/10.1016/j.catena.2015.10.015.
Semmel, A., 1968. Studien über den Verlauf jungpleistozäner Formung in Hessen. Kramer.
Semmel, A., 1989. The importance of loess in the interpretation of geomorphological processes and for dating in the federal Republic of Germany. Catena Suppl. 15, 179–188.
Smalley, I., 1966. The properties of glacial loess and the formation of loess deposits. J. Sediment. Petrol. 36, 669–676.
Smalley, I., 1995. Making the material: the formation of silt-sized primary mineral particles for loess deposits. QSR 14, 645–651.
Smalley, I., Marković, S.B., Svirčev, Z., 2011. Loess is [almost totally formed by] the accumulation of dust. QI 240 (1–2), 4–11. http://dx.doi.org/10.1016/j.quaint.2010.07.011.
Sprafke, T., Obreht, I., 2015. Loess: rock, sediment or soil – what is missing for its definition? QI http://dx.doi.org/10.1016/j.quaint.2015.03.033 (in press).

Terhorst, B., Appel, E., Werner, A., 2001. Palaeopedology and magnetic susceptibility of a loess–palaeosol sequence in southwest Germany. QI 76–77, 231–240. http://dx.doi.org/10.1016/S1040-6182(00)00105-1.

Thome, K.N., 1998. Einführung in das Quartär. Das Zeitalter der Gletscher, Berlin, Heidelberg, New York.

Thompson, R., Oldfield, F., 1986. Environmental Magnetism. 1st edition. Sydney, Boston.

Újvári, G., Kok, J.F., Varga, G., Kovács, J., 2016. The physics of wind-blown loess: implications for grain size proxy interpretations in Quaternary paleoclimate studies. Earth Sci. Rev. 154, 247–278. http://dx.doi.org/10.1016/j.earscirev.2016.01.006.

USS Working Group WRB, 2015. World Reference Base for Soil Resources 2014, update 2015, International soil classification system for naming soils and creating legends for soil maps. World Soil Resources Reports No. 106. FAO, Rome.

Van Vliet-Lanoë, B., 1989. Dynamics and extent of the Weichselian permafrost in western Europe (Substage 5E to stage 1). QI 3, 109–113. http://dx.doi.org/10.1016/1040-6182(89)90080-3.

Van Vliet-Lanoë, B., 1998. Frost and soils: implications for paleosols, paleoclimates and stratigraphy. Catena 34 (1–2), 157–183. http://dx.doi.org/10.1016/S0341-8162(98)00087-3.

Vandenberghe, J., 1985. Paleoenvironment and stratigraphy during the last glacial in the Belgian-Dutch border region. Quaternary Research 24 (1), 23–38 ISSN 0033-5894, http://dx.doi.org/10.1016/0033-5894(85)90081-X.

Vandenberghe, J., Nugteren, G., February 2001. Rapid climatic changes recorded in loess successions. Global and Planetary Change 28 (1–4), 1–9 ISSN 0921-8181, http://dx.doi.org/10.1016/S0921-8181(00)00060-6.

Vandenberghe, J., Zhisheng, A., Nugteren, G., Huayu, L., Van Huissteden, K., 1997. New absolute time scale for the Quaternary climate in the Chinese loess region by grain-size analysis. Geology 25 (1), 35–38. http://dx.doi.org/10.1130/0091-7613(1997)025<0035:NATSFT>2.3.CO;2.

Vandenberghe, J., Huijzer, B.S., Mücher, H., Laan, W., 1998. Short climatic oscillations in a western European loess sequence (Kesselt, Belgium). JQS 13 (5), 471–485.

Vlaminck, S., Kehl, M., Lauer, T., Shahriari, A., Sharifi, J., Eckmeier, E., Lehndorff, E., Khormali, F., Frechen, M., 2015. Loess-soil sequence at Toshan (Northern Iran): Insights into late Pleistocene climate change. QI http://dx.doi.org/10.1016/j.quaint.2015.04.028 (in press).

Wagenbreth, O., Steiner, W., 1990. Geologische Streifzüge: Landschaft und Erdgeschichte zwischen Kap Arkona und Fichtelberg. 4th edition. Leipzig.

Wagner, B., 2011. Spatial analysis of loess and loess-like sediments in the Weser-Aller catchment (Lower Saxony and Northern Hesse, NW Germany). E&G Quaternary Science Journal 60 (1), 27–46. http://dx.doi.org/10.3285/eg.60.1.00.

Wallinga, J., Murray, A., Wintle, A., 2000. The single-aliquot regenerative-dose (SAR) protocol applied to coarse-grain feldspar. Radiat. Meas. 32, 529–533. http://dx.doi.org/10.1016/S1350-4487(00)00091-3.

Wright, J.S., 2001. "Desert" loess versus "glacial" loess: quartz silt formation, source areas and sediment pathways in the formation of loess deposits. Geomorphology 36, 231–256.

Zagwijn, W.H., Van Staalduinen, C.J. (Eds.), 1975. Toelichtingen bij the geologische overzichtskarten van Nederland. Rijks Geologische Dienst, Haarlem.

Zech, M., Kraus, T., Meszner, S., Faust, D., 2013. Incorrect when uncorrected: reconstructing vegetation history using n-alkane biomarkers in loess-paleosol sequences – a case study from the Saxonian loess region, Germany. QI 296, 108–116.

Zeeden, C., Krauß, L., Kels, H., Lehmkuhl, F., 2016. Digital image analysis of outcropping sediments: comparison to photospectrometric data from Quaternary loess deposits at Şanovița (Romania) and Achenheim (France). QI http://dx.doi.org/10.1016/j.quaint.2016.02.047 (in press).

Zens, J., Zeeden, C., Römer, W., Fuchs, M., Lehmkuhl, F., 2016. Integrating age information from different localities for stratigraphic marker beds: discussion of the Eltville Tephra (Western Europe) age in review.